Comparison of Deterministic and Stochastic Models of the *lac* Operon Genetic Network

Michail Stamatakis* and Nikos V. Mantzaris
Department of Chemical and Biomolecular Engineering, Rice University, Houston, Texas 77005

ABSTRACT The *lac* operon has been a paradigm for genetic regulation with positive feedback, and several modeling studies have described its dynamics at various levels of detail. However, it has not yet been analyzed how stochasticity can enrich the system's behavior, creating effects that are not observed in the deterministic case. To address this problem we use a comparative approach. We develop a reaction network for the dynamics of the *lac* operon genetic switch and derive corresponding deterministic and stochastic models that incorporate biological details. We then analyze the effects of key biomolecular mechanisms, such as promoter strength and binding affinities, on the behavior of the models. No assumptions or approximations are made when building the models other than those utilized in the reaction network. Thus, we are able to carry out a meaningful comparison between the predictions of the two models to demonstrate genuine effects of stochasticity. Such a comparison reveals that in the presence of stochasticity, certain biomolecular mechanisms can profoundly influence the region where the system exhibits bistability, a key characteristic of the *lac* operon dynamics. For these cases, the temporal asymptotic behavior of the deterministic model remains unchanged, indicating a role of stochasticity in modulating the behavior of the system.

INTRODUCTION

The *lac* operon genetic switch is a paradigm for genetic regulation with positive feedback, and has been studied experimentally and theoretically for nearly half a century. Indeed, the operon concept, which pertains to a sequence of genes that function under the control of the same operator (1), was first introduced in 1960. The *lac* operon consists of three genes downstream of the *lac* promoter that encode for the proteins necessary for lactose metabolism. Specifically, *lacZ* encodes for β-galactosidase, which transforms lactose to the inducer allolactose; *lacY* encodes for LacY permease, which transports lactose into the cell; and *lacA* encodes for galactoside transacetylase (LacA), which transfers an acetyl group from acetyl-CoA to β-galactosides (2). Furthermore, upstream of the promoter, there exists the constitutively expressed *lacI* gene, which encodes for the LacI repressor protein.

The free LacI repressor is a tethered tetramer (dimer of dimers) (3) that has a high affinity for the *lacO* (*O1*) operator contained in the *lac* promoter. Therefore, in the absence of lactose, each LacI dimer binds to an operator and thus inhibits transcription of the *lacZ*, *lacY*, and *lacA* genes. LacI can also bind to pseudooperators that exist upstream (*O3*) and downstream (*O2*) of the promoter and create DNA loop structures (4–6). It has been suggested that binding of the LacI repressor to the pseudooperators results in a localization of LacI close to the main operator, thereby increasing its binding efficiency to the operator (7). Thus, more efficient suppression of the *lac* genes is attained.

However, if lactose is present in the extracellular medium, it gets transported into the cell, where one fraction is hydrolyzed to galactose and glucose and the other fraction is transformed to the inducer allolactose by β-galactosidase. The allolactose binds to the LacI repressor and forms a complex with reduced binding affinity to the operator. This process results in freeing the operator site(s). Induction of the LacI can also be achieved with a gratuitous inducer such as isopropyl-β-D-thiogalactopyranoside (IPTG), which does not require transformation by β-galactosidase. Instead, it can readily bind to the repressor with a stoichiometry of two IPTG molecules per LacI dimer (6).

Yet, for transcription of the *lac* operon genes to be initiated, the activator cAMP-CRP complex needs to bind to a sequence near the *lac* promoter, thereby enhancing the binding affinity of the RNA polymerase (8). High activator concentrations are brought about by low glucose concentrations. Hence, the *lac* operon genes are expressed only if the glucose concentration is low and simultaneously the lactose concentration is high. Therefore, glucose inhibits lactose metabolism in a dual manner: by reducing cAMP, and thus cAMP-CRP activator concentrations (catabolite repression); and by reducing inducer-allolactose concentrations, since it suppresses the *lac* operon genes (inducer exclusion).

Furthermore, since LacY facilitates lactose import, resulting in repressor inactivation, it follows that initial expression of the *lac* operon genes promotes further expression in an autocatalytic manner due to a positive feedback loop generated by the action of the permease. This positive genetic architecture is the cause of the experimentally observed all-or-none bistable response of the *lac* operon (9).

To reveal the role of the *lac* operon components, several experimental studies have introduced mutations to the promoter region or the coding sequences. Such mutations

Submitted February 28, 2008, and accepted for publication October 29, 2008.

*Correspondence: mstam@rice.edu

Editor: Arthur Sherman.

0006-3495/09/02/0887/20 $2.00

doi: 10.1016/j.bpj.2008.10.028

can result in strengthening, weakening, or completely eliminating some of the biomolecular interactions in the *lac* operon system. Thus, the negative feedback of glucose by the catabolite repression mechanism can be nullified by using a mutant promoter for the *lacZYA*, such as the *lac* UV5 promoter (10). On the other hand, the strength of repression can be altered by 1), introducing mutations to the *lacI* promoter, resulting in a different transcriptional rate of *lacI* (11,12); or 2), changing the binding affinity of LacI to the *lacO* or to the inducer IPTG by introducing mutations to the *lacI* gene (13–16). Moreover, the autocatalytic feedback can be suppressed by introducing mutations to the *lacY* gene, such that nonfunctional permease is produced (17).

The processes that take place during the expression of *lac* operon genes and the effect of mutations can be better understood by the use of mathematical modeling in close association with experiments. Therefore, soon after the introduction of the operon concept by Jacob et al. (1), modeling studies of the *lac* operon appeared in the literature.

By using a generic model for single gene induction, Griffith (18) showed that in a positive feedback loop architecture such as that exhibited in the *lac* operon, bistability is possible if more than one inducer molecule interact with the genetic locus. In Yagil and Yagil (19), a reaction scheme was proposed for the induction mechanism present in the *lac* operon, and it was shown experimentally that the Hill exponents for the induction of LacI have values close to 2, implying that two inducer molecules are required for this process.

Several subsequent models (20–24) utilized the reaction scheme by Yagil and Yagil (19) to model induction and catabolite repression in the case of multiple substrates, in different growth environments, or by taking into account membrane transport. In two milestone articles, Lee and Bailey (25,26) derived a detailed model that enabled them to investigate replication dynamics and polyploidity effects, and their coupling to the induction-repression mechanisms, transcription and translation. Laffend and Schuler extended the work of Lee and Bailey and showed that for high-copy plasmids, the ribosomes are not sufficient to translate the plasmid-derived mRNA into proteins (27–29).

Furthermore, Ray et al. (30) presented the first unified *lac* operon model that incorporated the role of the catabolite modulator factor in the regulation of transcription. Chung and Stephanopoulos (31) presented a minimal yet elegant *lac* operon model that takes into account repression and induction, as well as the positive feedback generated by the LacY permease. Straight and Ramkrishna (32) and Ramakrishna et al. (33), applied the cybernetic modeling approach and successfully predicted diauxic growth patterns and simultaneous consumption of substrates. Moreover, Wong et al. (34) developed a detailed mathematical model to study inducer exclusion, catabolite repression, and diauxic growth. Recently, Tian and Burrage (35) constructed a model that accounts for transcription and translation of the LacY permease and a green fluorescent protein reporter gene, and quantified the effect of different Hill coefficients for the transport of thiomethylgalactoside (TMG) on the LacY expression levels.

A class of models that takes into account transcriptional and translational delays has also been developed. Maffahy and Savev (36) showed that oscillatory behavior is possible in the *lac* operon for specific values of the transcriptional and translational delays. Yildirim and Mackey (37) developed a detailed *lac* operon model consisting of delay differential equations and successfully predicted the experimentally observed time course of β-galactosidase concentration and the bistable response of the *lac* operon.

Finally, Tanaka et al. (38) have developed a generic framework for transcriptional regulation that can also be used in the case of the *lac* operon system. The authors show that several published *lac* operon models can be reproduced by choosing the appropriate functional expressions in their framework.

None of the aforementioned works takes into account the inherent randomness of the biomolecular mechanisms of the *lac* operon system. However, studies have been published that incorporate stochastic effects on the mathematical description of the *lac* operon. Carrier and Keasling (39) used a unique mechanistic model to simulate the processes involved in *lacZ* gene expression, focusing on the effects of particular mRNA decay mechanisms. An adaptation of this model was later used by the same authors (40) to study the properties of gene expression in autocatalytic systems. It was shown that random cellular events govern the all-or-none phenomenon upon induction and that hysteretic responses can be observed. The authors also demonstrated that for homogeneous expression of the gene of interest, the inducer must not control the transport protein levels.

Mettetal et al. (41) started from a deterministic *lac* operon dynamic model (developed by Ozbudak (42)) into which white noise was added *a posteriori* (the ''Langevin approach'' (43)). The parameter values for the deterministic model were taken such that the model predictions agree with the dynamics of the experimentally measured cell population average. Furthermore, measurements of the noise around the steady state were used to estimate the parameters that determine the variance of the white noise terms. This model deals collectively with global noise, and also takes into account fluctuations in the green and red fluorescent protein concentrations. Mettetal et al. (41) showed that even though the deterministic model cannot fully capture the experimental observations, the stochastic model correctly does so after the noise characteristics have been adjusted to agree with the data.

Vilar et al. (44) derived a phenomenological deterministic model for the induction of the *lac* operon that predicts bistability and hysteresis. They incorporated stochasticity by converting the deterministic reaction terms into probability

transition rates and the concentrations into numbers of molecules. The stochastic model predicts random switches from the uninduced to the induced state. However, as the authors note, the model predicts that all cells eventually reach the induced state, unless one considers different growth rates for the induced versus the uninduced cells. Vilar et al. (44) pointed out that taking into account stochastic and population effects depends not only on the given system but also on the particular conditions.

Nevertheless, no study has compared corresponding deterministic and stochastic models to show whether the extra complexity reveals novel phenomena in the case of the *lac* operon system. Such phenomena have been demonstrated for other genetic networks, such as regulatory network motifs where a protein produced by transcriptional-translational bursts exerts positive or negative feedback to other promoters (45,46). In these systems, the random occurrence of biomolecular reactions results in temporal variability in the numbers of proteins. As a consequence, phenotypic variability is observed even when the average protein numbers stay constant (45). Further, it has been proposed that this variability may have a physiological significance, enhancing the viability of the cell population during environmental stress conditions or establishing cell population heterogeneity during cellular differentiation and development (47).

Phenotypic variability resulting from stochasticity has also been demonstrated in more complex systems. For the phage λ lysis-lysogeny decision circuit, Arkin et al. (48) showed that the inherent randomness of the biomolecular events coupled with the system's bistable response results in switching between different dynamical states. Consequently, the bacterial population splits into subpopulations of infected and uninfected cells. Deterministic models cannot account for this probabilistic switching, which is a key mechanism in the selection between alternative regulatory paths. For the same system, Hasty et al. (49) also showed that adding external noise into a deterministic model can induce switching or amplification effects.

The profound effect of stochasticity in creating de novo dynamical responses that cannot be predicted by deterministic modeling has been demonstrated in enzymatic futile cycles (50). Samoilov et al. (50) showed that in the absence of stochasticity the system is unable to exhibit bistable behavior, but when noise is added, stochastic switching (bistability) is observed.

Furthermore, Kepler and Elston (51) have developed exact stochastic models for several different genetic architectures, namely, a single gene without feedback, a single gene activating itself, and two genes mutually repressing each other. They have further derived approximations valid for low noise strength or rapid stochastic fluctuations, and by using the resulting approximate models, they were able to demonstrate bifurcations in the stochastic models, even when the corresponding deterministic equations remained unchanged.

In our study, we apply a different approach for the case of the *lac* operon system. Starting from the deterministic model, we compare its temporal asymptotic behavior with that of the corresponding exact stochastic model to show the effect of stochasticity. To this end, we first develop a reaction network that incorporates biological information about the *lac* operon. We derive a deterministic model and its corresponding stochastic model and analyze quantitatively the effect of biomolecular parameters on the behavior of each. We further compare the predictions of the deterministic and stochastic models. We reveal mechanisms that significantly influence the temporal asymptotic behavior of the stochastic, but not that of the deterministic, model. Since no approximations are imposed on either model other than those used in building the reaction network, this comparative approach can highlight the differences between the two models and thus elucidate the effect of stochasticity on the behavior of the *lac* operon system.

In the rest of this article, we discuss the assumptions used to build the *lac* operon reaction network and then derive the deterministic model, analyze its temporal asymptotic behavior, and perform sensitivity analysis with respect to parameters quantifying key biomolecular mechanisms. We further derive the stochastic model and use Gillespie's algorithm to simulate the stochastic dynamics (52). We present an in-depth analysis of the behavior of the system at different induction levels, highlighting the differences between the corresponding models. Finally, we summarize and discuss our results.

REACTION NETWORK

The molecular mechanisms included in our model appear schematically in Fig. 1. The constitutive expression of the *lacI* gene is modeled as the zeroth-order production of *lacI* mRNA (species M_R). The translation of *lacI* mRNA to LacI (species R) is modeled as a first-order catalytic reaction and the dimerization of LacI repressor (to form the dimer R_2) is assumed to follow second-order kinetics. Thus, production and dimerization of LacI is modeled by the reactions

$$\varnothing \xrightarrow{k_{sMR}} M_R \qquad \text{(i)}$$

$$M_R \xrightarrow{k_{sR}} M_R + R \qquad \text{(ii)}$$

$$2R \underset{k_{-2R}}{\overset{k_{2R}}{\rightleftarrows}} R_2. \qquad \text{(iii,iv)}$$

Wild-type LacI dimers can further assemble into a tethered tetramer (53). The tetramer can interact with pseudooperators and create loop structures (4) that result in tighter repression due to cooperativity between the (pseudo)operators (54). However, in this study, we are not concerned with the effects of cooperativity in the negative feedback due to repression; rather, our aim is to better understand the effect

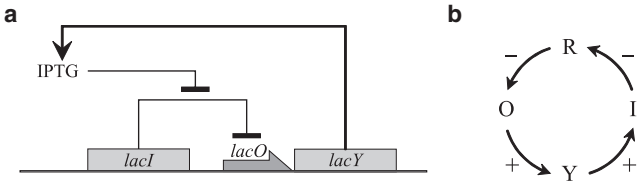

FIGURE 1 (*a*) Schematic representation of the interactions taken into account in the *lac* operon network. (*b*) Interaction diagram for the key species of the *lac* operon genetic switch (for species notation, see Table 1; + and − denote positive and negative feedback, respectively).

of stochasticity in the presence of positive feedback due to autocatalytic LacY production. Thus, we neglect tetramerization effects, assuming a mutant repressor that can form dimers but is unable to assemble into the tetrameric structure. Such mutants have been experimentally constructed (53,55,56) and are unable to create loop structures (4).

A LacI dimer is sufficient for specific binding to the operator sequence (6). However, a LacI monomer is unable to bind *lacO* and exert any repressive effect (53). Thus, we assume that the repressor dimer binds to the operator (denoted as species O) with a one-to-one stoichiometry. Under these assumptions, repressive action is expressed as

$$R_2 + O \underset{k_{-r}}{\overset{k_r}{\rightleftarrows}} R_2O. \qquad \text{(v, vi)}$$

Furthermore, induction of the *lac* operon is assumed to take place with a gratuitous inducer, such as TMG or IPTG (denoted as species I), which does not require transformation by β-galactosidase. Thus, the dynamics of this enzyme are not taken into account. Equilibrium dialysis studies have shown that IPTG binds strongly to the LacI tetramer with a stoichiometry that varies depending on the conditions but reaches a value of 4 at high temperatures (one IPTG molecule per LacI monomer (57)). In a LacI tetramer, inducer binding to each LacI dimer can be considered separately, because the only allosteric changes in the repressor molecule occur between chains in a dimer (58). Hence, the interaction of a LacI dimer with two IPTG molecules is adequate to describe the mechanism of allosteric regulation, and thus we use this mechanism in our model. We assume cooperative binding, with a Hill coefficient equal to 2 for the binding of inducer to repressor. Therefore, the phenomenon can be modeled as one third-order reaction:

$$2I + R_2 \underset{k_{-dr1}}{\overset{k_{dr1}}{\rightleftarrows}} I_2R_2, \qquad \text{(vii, viii)}$$

where (vii) is the forward reaction. Furthermore, IPTG can also bind to the repressor-operator complex, thereby freeing the operator from the repressor:

$$2I + R_2O \underset{k_{-dr2}}{\overset{k_{dr2}}{\rightleftarrows}} I_2R_2 + O. \qquad \text{(ix,x)}$$

Experimental studies have shown different Hill coefficient values, ranging from 1 to 3 (19). Cooperativity values depend on whether the inducer binds free repressor versus repressor-operator complex, whether it can be altered by mutations, and whether it depends on environmental conditions such as pH (19,59,60). Furthermore, it has been proposed that cooperativity can be explained by the formation of DNA loop structures (61). However, in our study, we are not concerned with such structures, and thus we make the simplifying assumption that cooperativity is equal to 2, as suggested by the reaction scheme of Yagil and Yagil (19).

Note that the reversible reactions (v, vi), (vii, viii) and (ix, x) are linearly dependent, and thus the equation for their dissociation constants holds:

$$\frac{k_r}{k_{-r}} \cdot \frac{k_{-dr1}}{k_{dr1}} \cdot \frac{k_{dr2}}{k_{-dr2}} = 1. \qquad (1)$$

Equation 1 essentially expresses Hess's law for the Gibbs free energy applied to the set of chemical equilibria v–x (see Appendix 1).

For the *lacY* transcription, we use a catalytic first-order reaction where the rate of *lacY* mRNA (species M_Y) production depends on the concentration of the free operator. We assume that the transcription of *lacY* is driven by a mutant promoter that is insensitive to glucose, such as the UV5, and thus the catabolite repression effects are neglected:

$$O \overset{k_{s1MY}}{\rightarrow} O + M_Y \qquad \text{(xi)}$$

Leak transcription of *lacY* is modeled by the reaction

$$R_2O \overset{k_{s0MY}}{\rightarrow} R_2O + M_Y. \qquad \text{(xii)}$$

Translation of *lacY* to LacY (species Y) is modeled as a first-order reaction:

$$M_Y \overset{k_{sY}}{\rightarrow} M_Y + Y. \qquad \text{(xiii)}$$

The facilitated transport of IPTG from the extracellular to the cytosolic space was assumed to follow Michaelis-Menten kinetics (62). The LacY permease plays the role of the enzyme and the extracellular IPTG (I_{ex}) that of the substrate:

$$Y + I_{ex} \underset{k_{-p}}{\overset{k_p}{\rightleftarrows}} YI_{ex} \overset{k_{ft}}{\rightarrow} Y + I, \qquad \text{(xiv–xvi)}$$

where (xiv) is the reaction k_p and (xvi) corresponds to reaction k_{ft}. Moreover, the free diffusion of IPTG through the membrane was described by two first-order reactions with the exact same kinetic constants:

$$I_{ex} \underset{k_t}{\overset{k_t}{\rightleftarrows}} I. \qquad \text{(xvii, xviii)}$$

Degradation reactions were modeled using the following assumptions. Since the operator does not degrade, neither does the operator-repressor complex degrade (the repressor has to dissociate first and then degrade). Also, IPTG is

nonmetabolizable, so it does not degrade itself, but the repressor-inducer complex degrades to give two IPTG molecules. Similarly, the permease inducer complex degrades in the interior of the cell to give one IPTG molecule. We further assume that the repressor does not degrade when bound to the operator. We have not found experimental data to support this assumption, but one expects that the chaperones/proteases would not be able to access the repressor when bound to DNA due to steric hindrance effects. Last, all degradation reactions are assumed to follow first-order kinetics:

$$M_R \xrightarrow{\lambda_{MR}} \varnothing \quad \text{(xix)}$$

$$M_Y \xrightarrow{\lambda_{MY}} \varnothing \quad \text{(xx)}$$

$$R \xrightarrow{\lambda_R} \varnothing \quad \text{(xxi)}$$

$$R_2 \xrightarrow{\lambda_{R2}} \varnothing \quad \text{(xxii)}$$

$$Y \xrightarrow{\lambda_Y} \varnothing \quad \text{(xxiii)}$$

$$YI_{ex} \xrightarrow{\lambda_{YIex}} I \quad \text{(xxiv)}$$

$$I_2R_2 \xrightarrow{\lambda_{I2R2}} 2I. \quad \text{(xxv)}$$

We further neglected cell growth and division, assuming that the total DNA and therefore the operator concentration in the cell, remain constant, and that the cell volume remains constant. This simplifying assumption allows us to analyze in isolation the genuine effects of stochasticity in biomolecular reactions. Cell growth and division have their own effects, analysis of which is not the objective of this study.

In summary, the reaction network from which the two corresponding models will be derived consists of reactions (i–xxv). Species notation is summarized in Table 1 and the values of the kinetic constants and other parameters are shown in Table 2. Most of the parameter values were determined from the literature. In cases where no data could be found, estimated values were used such that the results of the simulations compare well with experimental observations.

To obtain a better understanding of the model and to gain insight into the effect of various mechanisms on its behavior, we first analyze the deterministic equations arising from the reaction network and then investigate the effect of stochasticity.

TABLE 1 Symbols used for the *lac* operon species

Symbol	Species denoted
M_R	LacI repressor mRNA
R	LacI repressor monomer
R_2	LacI repressor dimer
O	*lacO* operator
R_2O	Repressor-operator complex
I	Intracellular inducer IPTG
I_{ex}	Extracellular inducer IPTG
I_2R_2	Repressor-inducer complex
M_Y	LacY permease mRNA
Y	LacY permease
YI_{ex}	Permease-inducer complex
$\varnothing$	Generic source or sink

DETERMINISTIC MODEL

The deterministic model consists of the mass balances for the interacting species subject to conservation conditions. Concentration of species X is denoted as [X] (for species notation, see Table 1). The total operator concentration ($[O]_T$) is constant and equal to the free operator concentration plus that bound to the repressor.

$$[O]_T = [O] + [R_2O] \quad (2)$$

Utilizing the above relation, the mass balances are written as

$$\frac{d[M_R]}{dt} = k_{sMR} - \lambda_{MR}\cdot[M_R] \quad (3)$$

$$\frac{d[R]}{dt} = k_{sR}\cdot[M_R] - 2\cdot k_{2R}\cdot[R]^2 + 2\cdot k_{-2R}\cdot[R_2] - \lambda_R\cdot[R] \quad (4)$$

$$\frac{d[R_2]}{dt} = k_{2R}\cdot[R]^2 - k_{-2R}\cdot[R_2] - k_r\cdot[R_2]\cdot[O] + k_{-r}\cdot\left([O]_T - [O]\right) - k_{dr1}\cdot[R_2]\cdot[I]^2 + k_{-dr1}\cdot[I_2R_2] - \lambda_{R2}\cdot[R_2] \quad (5)$$

$$\frac{d[O]}{dt} = -k_r\cdot[R_2]\cdot[O] + k_{-r}\cdot\left([O]_T - [O]\right) + k_{dr2}\cdot\left([O]_T - [O]\right)\cdot[I]^2 - k_{-dr2}\cdot[O]\cdot[I_2R_2] \quad (6)$$

$$\frac{d[I]}{dt} = -2\cdot k_{dr1}\cdot[R_2]\cdot[I]^2 + 2\cdot k_{-dr1}\cdot[I_2R_2] - 2\cdot k_{dr2}\cdot\left([O]_T - [O]\right)\cdot[I]^2 + 2\cdot k_{-dr2}\cdot[O]\cdot[I_2R_2] + k_{ft}\cdot[YI_{ex}] + k_t\cdot([I_{ex}] - [I]) + 2\cdot\lambda_{I2R2}\cdot[I_2R_2] + \lambda_{YI_{ex}}\cdot[YI_{ex}] \quad (7)$$

$$\frac{d[I_2R_2]}{dt} = k_{dr1}\cdot[R_2]\cdot[I]^2 - k_{-dr1}\cdot[I_2R_2] + k_{dr2}\cdot\left([O]_T - [O]\right)\cdot[I]^2 - k_{-dr2}\cdot[O]\cdot[I_2R_2] - \lambda_{I2R2}\cdot[I_2R_2] \quad (8)$$

$$\frac{d[M_Y]}{dt} = k_{s0MY}\cdot\left([O]_T - [O]\right) + k_{s1MY}\cdot[O] - \lambda_{MY}\cdot[M_Y] \quad (9)$$

TABLE 2 Parameters of the *lac* operon reaction model

Symbol	Value	Units	Description
$V_{E.\ coli}$	8×10^{-16}	L	*E. coli* volume*
O_T	1	(copy number)	operator content ($[O]_T \approx 2.08$ nM)
k_{sMR}	0.23	$nM \cdot min^{-1}$	*lacI* transcription rate†
k_{sR}	15	min^{-1}	LacI monomer translation rate constant†
k_{2R}	50	$nM^{-1} \cdot min^{-1}$	LacI dimerization rate constant‡
k_{-2R}	10^{-3}	min^{-1}	LacI dimer dissociation rate constant‡
k_r	960	$nM^{-1} \cdot min^{-1}$	association rate constant for repression§
k_{-r}	2.4	min^{-1}	dissociation rate constant for repression§
k_{dr1}	3×10^{-7}	$nM^{-2} \cdot min^{-1}$	association rate constant for 1st derepression mechanism ¶
k_{-dr1}	12	min^{-1}	dissociation rate constant for 1st derepression mechanism ¶
k_{dr2}	$3 \cdot 10^{-7}$	$nM^{-2} \cdot min^{-1}$	association rate constant for 2nd derepression mechanism‖
k_{-dr2}	$4.8 \cdot 10^{3}$	$nM^{-1} \cdot min^{-1}$	dissociation rate constant for 2nd derepression mechanism‖
k_{s1MY}	0.5	min^{-1}	*lacY* transcription rate constant†
k_{s0MY}	0.01	min^{-1}	leak *lacY* transcription rate constant†
k_{sY}	30	min^{-1}	*lacY* translation rate constant†
k_p	0.12	$nM^{-1} \cdot min^{-1}$	LacY-IPTG$_{ex}$ association rate constant**
k_{-p}	0.1	min^{-1}	LacY-IPTG$_{ex}$ dissociation rate constant**
k_{ft}	6.10^{4}	min^{-1}	IPTG-facilitated transport constant**
k_t	0.92	min^{-1}	IPTG passive diffusion constant**
λ_{MR}	0.462	min^{-1}	*lacI* mRNA degradation constant†
λ_{MY}	0.462	min^{-1}	*lacY* mRNA degradation constant†
λ_R	0.2	min^{-1}	repressor monomer degradation constant†
λ_{R2}	0.2	min^{-1}	LacY degradation constant†
λ_Y	0.2	min^{-1}	LacY-inducer degradation constant†
λ_{YIex}	0.2	min^{-1}	LacY-inducer degradation constant†
λ_{I2R2}	0.2	min^{-1}	repressor-inducer degradation constant†

E. coli volume is roughly the average between 6×10^{-16} and 9.8×10^{-16} (75).

†Parameters for which experimental values could not be determined from the literature were estimated so that the species concentrations were within reasonable limits. Thus, 1), the ratio of the intracellular with respect to the extracellular IPTG concentration must be on the order of 26~400 (62); and 2), at the fully induced state there are roughly 400 ± 200 nM LacY permease or, equivalently, 200 ± 100 LacY permease molecules (63). We used this information to estimate the production and degradation rates of M_Y and Y. Furthermore, 3), the total concentration of dimeric repressor in the cell is estimated to be 20 nM or, equivalently, 10 repressor dimers (19,65); thus, we estimated production and degradation constants for the species M_R, R, R_2, and I_2R_2 that agree with this data. The order of magnitude for the production and degradation rates was taken such that upon step changes of $[I_{ex}]$ the system will respond within a reasonable *E. coli* division time (~40 min maximum).

‡We could not find experimental data for the dimerization rate or thermodynamic constant, so these values are estimated and express fast and tight dimerization.

§The equilibrium constant k_{-r}/k_r is ~10^{-13}–10^{-11} M (76–78). The half-life for dissociation of operator DNA fragments from the repressor has been reported as ~30–49 s (76,79). We take the dissociation rate $k_{-r} = 2.4\ min^{-1}$, $k_r = 960\ nM^{-1} \cdot min^{-1}$ (thus, $k_{-r}/k_r = 2.5 \times 10^{-12}$).

¶The equilibrium constant k_{-dr1}/k_{dr1} is $40 \times 10^{-12}\ M^2 = 4 \times 10^{7}\ nM^2$ (19). The dissociation rate constant k_{-dr1} is $0.2\ s^{-1} = 12\ min^{-1}$ (80).

‖For the association constant for the second derepression mechanism (k_{dr2}), we used a value equal to that of the first mechanism (k_{dr1}). The value for the dissociation constant (k_{-dr2}) was calculated using Eq. 1.

**For the Michaelis-Menten scheme, $(k_{-p} + k_{ft})/k_p = 5 \times 10^5$ nM, $k_{ft} = 6 \times 10^4\ min^{-1}$ and k_t reported for TMG is $0.92\ min^{-1}$ (31,62,63). Thus, we use $k_{-p} = 0.1\ min^{-1}$, $k_p = 0.12\ nM^{-1}\ min^{-1}$.

$$\frac{d[Y]}{dt} = k_{sY} \cdot [M_Y] + (k_{ft} + k_{-p}) \cdot [YI_{ex}] - k_p \cdot [Y] \cdot [I_{ex}] - \lambda_Y \cdot [Y] \quad (10)$$

$$\frac{d[YI_{ex}]}{dt} = -(k_{ft} + k_{-p}) \cdot [YI_{ex}] + k_p \cdot [Y] \cdot [I_{ex}] - \lambda_{YIex} \cdot [YI_{ex}]. \quad (11)$$

Temporal asymptotic behavior

To study the behavior of the *lac* operon as predicted by the deterministic model, we will first solve for the steady-state concentrations of the species. The extracellular IPTG concentration ($[I_{ex}]$) will be used as the main bifurcation parameter, since it can be experimentally varied, hence rendering possible the connection between theory and experiment. Furthermore, it will be discussed how key parameters linked to biomolecular mechanisms affect the system's behavior. The primary observation in the system will be the total LacY concentration (namely $[Y] + [YI_{ex}]$), since it can be measured experimentally with the use of reporter proteins or Western blot analysis.

In Fig. 2 *a*, the steady-state concentrations of total LacY are plotted with respect to the $[I_{ex}]$. All one-parameter bifurcation diagrams were computed by performing pseudo-arc length continuation for the steady states of Eqs. 3–11. We observe that for low or high IPTG concentrations, only one stable steady state exists. Within the range $[I_{ex}] \approx 24.2$–$32.4\ \mu M$, two branches of stable steady states exist, separated by a branch of unstable steady states. This bistable response can be explained in terms of the positive feedback

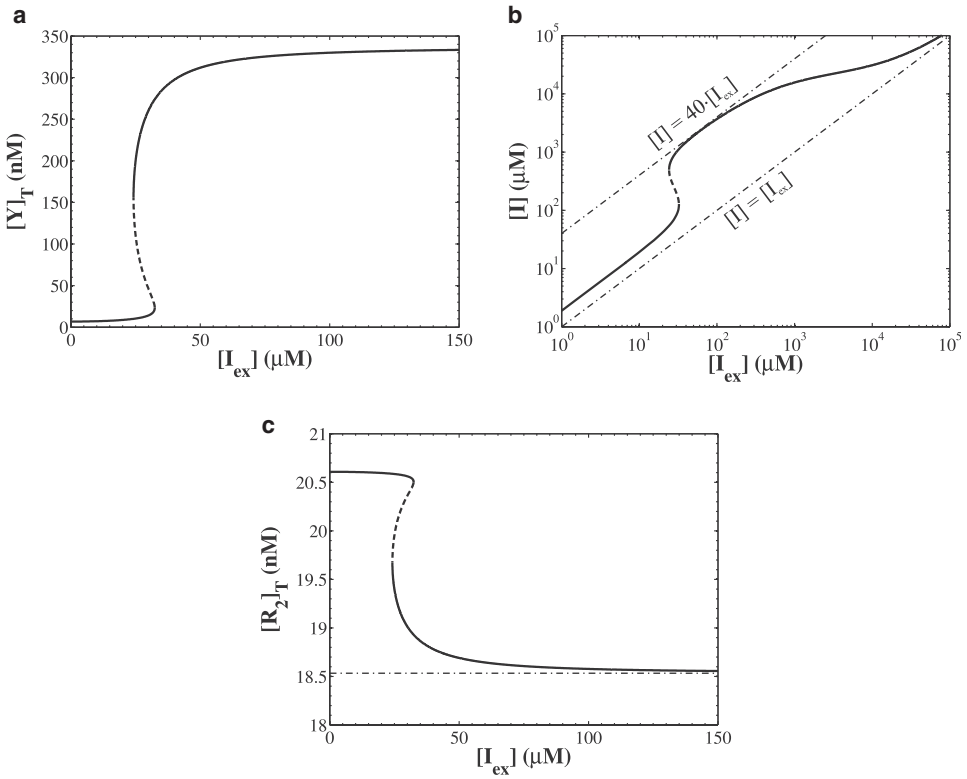

FIGURE 2 Bifurcation diagrams with respect to the extracellular IPTG concentration, $[I_{ex}]$, for (*a*) the total LacY concentration, (*b*) the intracellular IPTG concentration, and (*c*) the total repressor concentration (the dot-dashed line corresponds to the limiting $[R]_T$ as calculated from Eq. S46). Solid lines represent stable and dashed lines unstable steady states. For a complete list of parameters, see Table 2.

architecture of the *lac* operon system. For low concentrations of $[I_{ex}]$, a minimal amount of LacY is produced, so the *lacY* gene essentially remains turned off (left monostable regime). For intermediate $[I_{ex}]$ (bistable region), if the initial content of LacY in the cell is low, then it will be impossible to turn on the *lacY* gene. However, if the initial LacY content is high enough, the *lacY* gene will be turned on and remain so, as a consequence of the facilitated transport of inducer into the cytosol. Finally, for very high $[I_{ex}]$, the *lacY* gene cannot be turned off. Even if the initial LacY was zero, the IPTG that freely diffuses in this case is sufficient to turn on the gene and activate the positive feedback loop. Thereafter, the facilitated transport due to the LacY permease dominates, the cell always reaches the induced state, and bistability vanishes. Such threshold phenomena in the dynamics of induction have also been observed experimentally (9,63) and are commonly referred to as ''all-or-none'' phenomena.

The facilitated IPTG transport, occurring after induction, also generates a bistable response for the intracellular IPTG (Fig. 2 *b*). Moreover, the plot of intracellular IPTG with respect to extracellular IPTG reveals a saturation effect: for high induction levels, the total LacY that exists in the cell remains mostly in the bounded form, YI_{ex}, (for a mathematical proof of this statement, see ''Limiting relations for the deterministic model for high inducer concentrations'' in Supporting Material). Thus, the remaining free LacY is not sufficient to transport IPTG into the cell, and consequently, no facilitated diffusion can take place. This explains the drop in the rate at which the intracellular IPTG concentration increases (after $[I_{ex}] = 100\ \mu M$). On the other hand, for small induction levels, the intracellular and the extracellular IPTG will also be approximately equal, since only a leak amount of LacY exists to facilitate the IPTG transport. Between the two limiting cases, there is a region where the intracellular IPTG concentration is roughly 40-fold higher than the extracellular concentration. This value is within the range measured for other galactosides: 26 for TPG, 65 for TMG, and 400 for TDG (62), and it can be increased by (results not shown) 1), faster LacY production or higher $[O]_T$; 2), faster association of the extracellular to the LacY permease (higher values for k_p); and 3), faster facilitated transport (higher values for k_{ft}).

Furthermore, the total repressor dimer concentration $[R_2]_T = [R_2] + [R_2O] + [I_2R_2]$ also assumes limiting values for low and high induction levels (Fig. 2). Between the two limits (low and high induction) there exists a region where bistability is observed for the total [LacI]. The prediction of this bistable response for $[R]_T$ is a novel feature of our model that results from the incorporation of LacI dynamics into the reaction network. Previous models neglect LacI dynamics and assume a nonregenerative repressor pool ($[R_2]_T$ = constant), which is used by the cell-to-block *lacY* transcription. When IPTG is added, it binds with a high affinity to the repressor, brings about the depletion of the available free LacI, and results in the cessation of *lacY*

suppression. Therefore, the ''switch-on'' mechanism in those models is based on the depletion of LacI from the nonregenerative repressor pool. On the contrary, in our model, we have relaxed the assumption of constant total repressor concentration. In this case, higher induction levels result in higher repressor-inducer complex concentrations (I_2R_2) and lower repressor-operator complex concentrations (R_2O). Since both the free repressor and the complex degrade at the same rate, but the R_2O complex does not degrade at all, it follows that higher IPTG concentrations lead to a higher net loss of repressor. Thus, in our model, the ''switch-on'' mechanism is based on the differential degradation of the repressor-inducer and repressor-operator complexes.

Accordingly, Fig. 3 *a* reveals that the degradation rate of the repressor-inducer complex (λ_{I2R2}) is a key parameter affecting the region of the parameter space where bistability is observed. The plot presents a two-parameter bifurcation diagram for the turning points with respect to λ_{I2R2} and the extracellular IPTG concentration. This and all subsequent two-parameter bifurcation diagrams were computed using zeroth-order continuation to the formulation that characterizes the turning-point bifurcation (Eqs. 2.27–2.29 in Salinger et al. (64)). We observe that as λ_{I2R2} tends toward zero, the bistable regime shifts progressively to larger extracellular IPTG concentrations. For the limiting case where the complex does not degrade at all, the system becomes noninducible.

There are several other parameters that have a significant effect on the region of bistability and also can be experimentally manipulated to make possible the connection with experiments. Thus, in Fig. 3 *b*, the effect of the *lacI* transcription rate (k_{sMR}) is shown. The bistable regime is enclosed in the spindle-shaped area, and it is apparent that higher *lacI* transcription rates result in shifting the bistable regime to higher extracellular inducer concentrations until the system becomes so repressed that bistability is destroyed. Qualitatively identical is the effect of the translation rate k_{sR} (Fig. S1 *a*). This effect is due to the higher LacI concentrations brought about by higher transcription (or translation) rates. In this case, induction will need more IPTG to inactivate the repressor, and thus switching from the uninduced to the induced state occurs at a higher extracellular [IPTG].

The region of bistability is also greatly affected by binding of the repressor to the inducer (Fig. 3 *c*). For higher values of the inducer unbinding constant (k_{-dr1}), the bistable regime shifts toward higher extracellular IPTG concentrations. This effect results from weaker binding of the inducer to the repressor and, thus, less potent inductive action. Consequently, the system needs higher inducer concentrations to reach the induced state. In contrast, binding of the repressor to the operator follows the opposite trend: weaker repressor-operator binding (higher k_{-r} values) results in less potent repressive action. Thus, the system can be induced with lower inducer concentrations and the bistable regime shifts to lower extracellular [IPTG] (Fig. S1 *b*). Both of these mechanisms can be experimentally manipulated by introducing mutations to the *lacI* gene that affect the binding affinities of LacI to *lacO* or IPTG.

It is interesting to note that the total LacY concentration at maximal induction is not affected by either of the aforementioned parameters (namely, k_{sMR}, λ_{I2R2}, and k_{dr1}/k_{-dr1} or

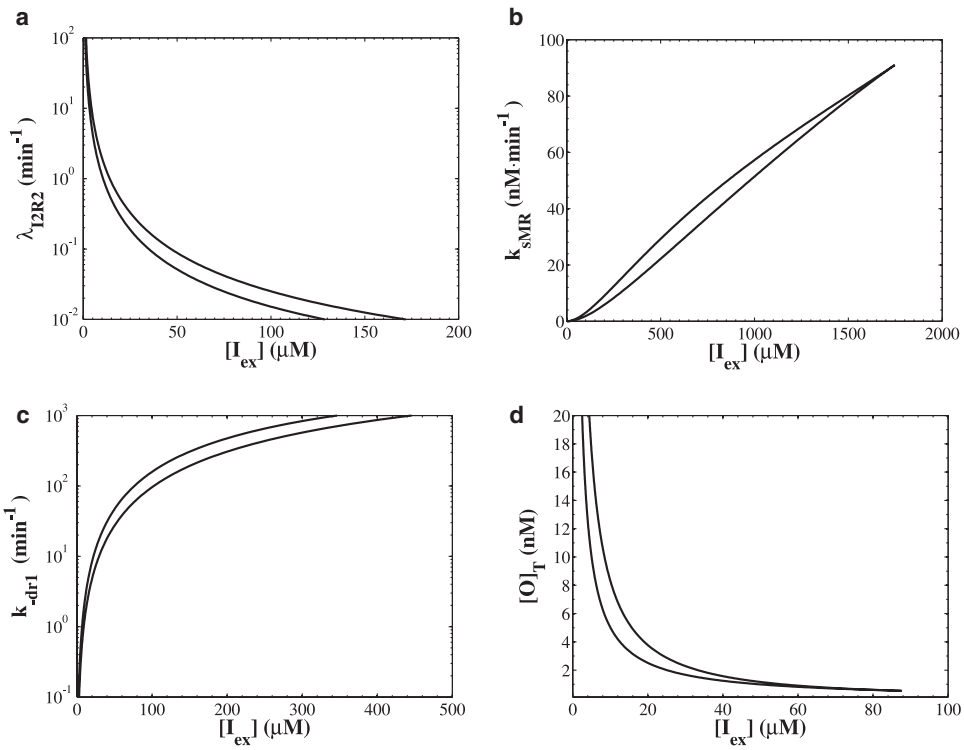

FIGURE 3 Two parameter bifurcation diagrams for the turning points showing the effect of several biomolecular parameters on the bistable regime (enclosed between the curves). Shown are the effects of repressor-inducer complex degradation rate (*a*), *lacI* transcription rate (*b*), repressor-inducer dissociation rate (*c*), and total operator concentration (*d*). Unless otherwise noted, parameters are as given in Table 2.

k_r/k_{-r}). In fact, the maximal total LacY concentration can be calculated as (see Eq. S41)

$$\lim_{[I_{ex}]\to\infty}[Y]_T = \frac{k_{sY}}{\lambda_{YIex}}\cdot\frac{k_{s1MY}}{\lambda_{MY}}\cdot[O]_T. \quad (12)$$

As expected, this shows that the repressor serves only to turn a gene on and off, and does not affect transcription or translation rates of the fully induced state. On the other hand, the maximal $[Y]_T$ scales linearly with the total operator concentration $[O]_T$, a parameter directly related to copy number of the genetic material. Furthermore, the total operator concentration strongly affects the extent of the bistable region. As shown in Fig. 3 *d*, higher $[O]_T$s result in initially wider and subsequently narrower bistable regions, shifted to smaller extracellular IPTG concentrations $[I_{ex}]$. These effects are observed because of the strengthening of the positive feedback loop.

Alternative derepression mechanisms

The results presented thus far pertain to the case where both derepression mechanisms are included in the model (reversible reactions vii, viii and ix, x). It is of experimental interest to demonstrate possible differences in the behavior of the system that arise if only one or the other mechanism is functional. Such effects were studied in the temporal asymptotic limit, as well as in the transient behavior, by keeping the thermodynamic constants fixed and changing the rates of association and dissociation. For clarity, we will refer to reactions (vii, viii) as the mechanism in which the inducer binds to the free repressor, and to reactions (ix, x) as the mechanism in which the inducer binds to the repressor-operator complex.

Thus, the mechanism in which the inducer binds to the repressor-operator complex was found to destroy bistability for slower repressor-operator association and dissociation rates (Fig. 4 *a*), which combines three bifurcation diagrams for $[Y]_T$ versus $[I_{ex}]$ for three different rates. Furthermore, for this case, faster induction is observed transiently (Fig. 4 *b*), because once the inducer has freed the operator from the repressor (fast process), the free repressor can bind again to the operator with a lower rate. The lower this rate is, the faster the induction. On the other hand, the mechanism in which the inducer binds to the free repressor does not result in changes of the bifurcation structure, but it results in slower induction, since in this case the repressor must first dissociate from the operator and then bind to the inducer (Fig. S1 *c*).

Furthermore, for slower repressor-inducer association and dissociation rates, the mechanism in which the inducer binds to the free repressor results in shifting of the bistable regime to higher I_{ex} concentrations and delayed induction (Fig. 4, *c* and *d*). Both effects can be attributed to repressor-inducer complex degradation occurring faster than repressor-inducer association. Thus, the system needs higher IPTG concentrations to effectively suppress the repressive action.

Finally, for slower repressor-operator complex-inducer association and dissociation rates, the mechanism in which the inducer binds to the repressor operator complex results in a broadening, but not significant shifting, of the bistable regime and slower induction (Fig. 4, *e* and *f*). These effects may be attributed to the progressively more significant contribution of I_2R_2 degradation. This I_2R_2 ''sink'' results in shifting the equilibrium of reactions (ix, x) to the right, thereby enhancing the positive feedback effect and broadening the bistable regime.

For the case the two mechanisms coexist, lower association and dissociation rates for any equilibrium produce no appreciable effects because the system can preferentially use one or the other derepression mechanism, thereby making up for the lower rates of the other.

STOCHASTIC MODEL

The deterministic model gave significant insight into the behavior of the *lac* operon system. However, there are indications that for this system stochasticity may be considerable. In particular, some of the interacting species have low copy numbers: the number of LacY permease molecules at the fully induced state is ~200 ± 100 (63); the total number of repressor molecules in the cell is estimated to be 10 dimeric copies per gene (19,65), which can be increased 10- or 20-fold as a result of the i^q mutation (65,66); and the operator copy number is 1 (or 2 during DNA duplication) for a chromosomal *lacO*. In view of these experimental data, it is reasonable to study the effects of stochasticity on network behavior by comparing the predictions of the deterministic model to those of the corresponding stochastic model.

The stochastic model derived from our reaction network consists of the chemical Master-equation (M-equation) (52)

$$\frac{\partial P(\mathbf{x},t|\mathbf{x}_0,t)}{\partial t} = \sum_{j=1}^{m}\left[\alpha_j(\mathbf{x}-\mathbf{v}_j)\cdot P(\mathbf{x}-\mathbf{v}_j,t|\mathbf{x}_0,t) - \alpha_j(\mathbf{x})\cdot P(\mathbf{x},t|\mathbf{x}_0,t)\right]. \quad (13)$$

For our system, the M-equation is impossible to solve analytically (however, see McQuarrie (67) for an excellent review of M-equations for simple chemical systems and their solutions). Thus, we used the direct method of Gillespie's algorithm (52,68) to simulate the stochastic dynamical behavior of the *lac* operon system. The state vector containing numbers of molecules for each species is $\mathbf{x} = \{M_R, R, R_2, O, R_2O, I, I_2R_2, M_Y, Y, YI_{ex}\}$, and we have $n = 10$ species participating in $m = 25$ reactions. The reactions' propensity functions, $\alpha_j(\mathbf{x}) = c_j \cdot h_j(\mathbf{x})$, $j = 1, 2, \ldots, m$, can be calculated given the macroscopic kinetic constants of Table 2, and are presented in Table 3. The vectors, $\mathbf{v}_j$, denote the change in the number of molecules for each species, e.g., for reaction ix, $\mathbf{v}_9 = \{0, 0, 0, 1, -1, -2, 1, 0, 0, 0\}$.

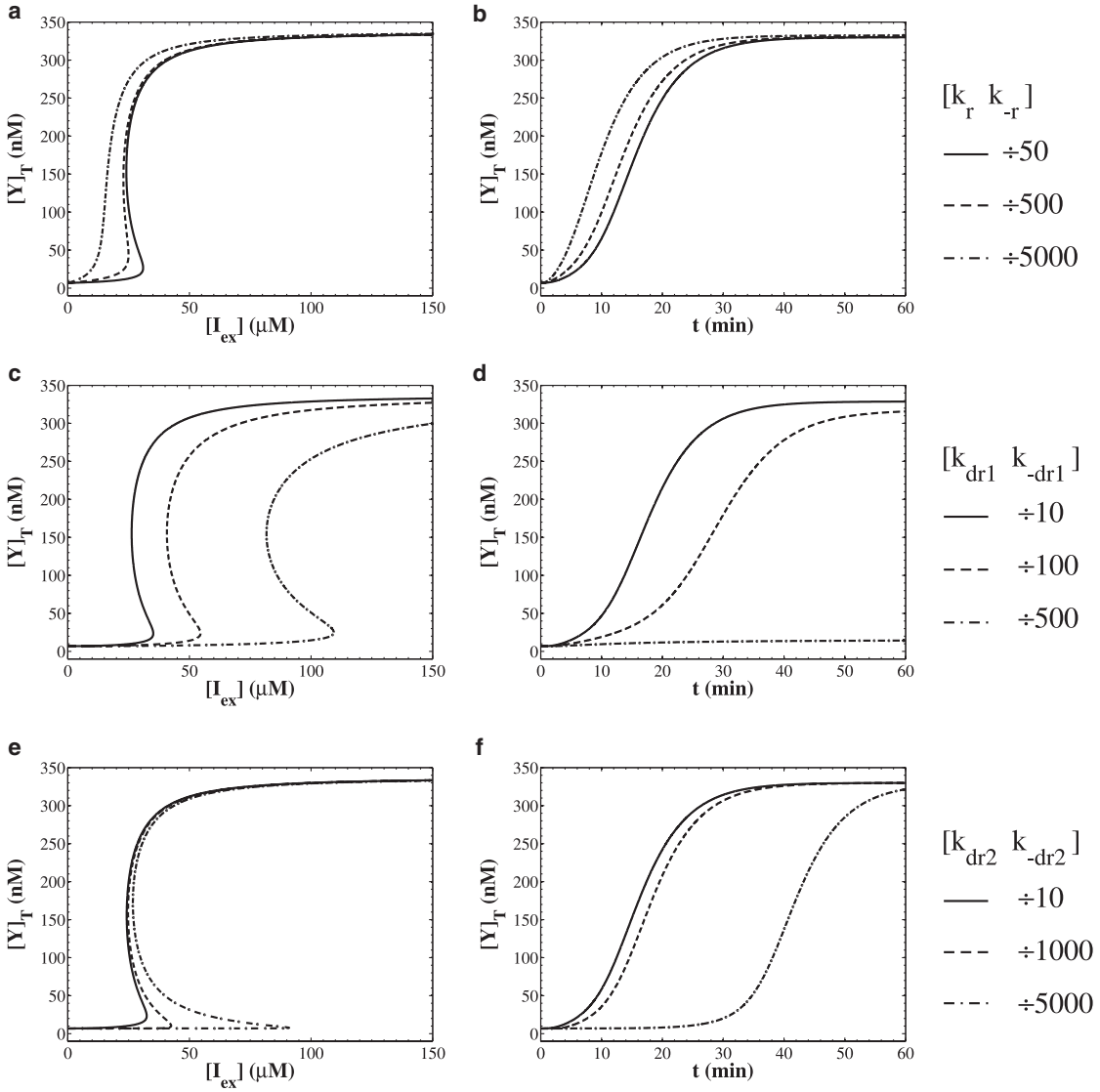

FIGURE 4 Transient and asymptotic effects of the alternative derepression mechanisms. (*a* and *b*) The mechanism where the inducer binds to the repressor-operator complex (thus, for the other mechanism, k_{dr1} and k_{-dr1} are both zero): loss of bistability and faster induction in the case of slower repressor-operator association and dissociation rates. [k_r, k_{-r}] ÷ 50 denotes that both k_r and k_{-r} have values 50-fold lower than those given in Table 2. (*c* and *d*) The mechanism where the inducer binds the free repressor (thus, k_{dr2} and k_{-dr2} are both zero): Shift of the bistable regime and slower induction for the case of slower repressor-inducer association and dissociation rates. The time course for [k_{dr1}, k_{-dr1}] ÷ 500 finally approaches the lower steady state. (*e* and *f*) The mechanism where the inducer binds to the repressor-operator complex (thus, k_{dr1} and k_{-dr1} are both zero), leading to broadening of the bistable regime and slower induction in the case of slower repressor operator complex-inducer association and dissociation rates. Parameters are as in Table 2, except as noted. For all induction transients, the initial condition is the corresponding steady state for $[I_{ex}] = 0$ μM, and at $t = 0$ min, an extracellular IPTG concentration of $[I_{ex}] = 100$ μM is imposed.

From the simulated sample paths, one can estimate the mean and standard deviation of the total LacY concentration $[Y]_T$ for a range of extracellular [IPTG] and compare them to the deterministic steady-state predictions (Fig. 5; for details about the simulation scheme used, sampling method, and te calculation of statistics, see Appendix 2). We observe that there is a significant difference between the average (stochastic) and the steady-state (deterministic) concentrations within a wide range of $[I_{ex}]$. Furthermore, as $[I_{ex}]$ increases, the standard deviations become markedly high because of the positive feedback loop: the total LacY concentration jumps between a maximal value corresponding to the induced state and a minimal value corresponding to the uninduced state. This observation implies that the marginal probability mass function (PMF) for $[Y]_T$ contains important information that cannot be captured with just the average and the standard deviation. Furthermore, the marginal PMF for $[Y]_T$ is a sufficiently good observable, since LacY is the key species of the positive feedback mechanism. Thus, we do not need to consider the entire 10-dimensional PMF for all the species (a task that would also be impossible due to computer memory limitations; see section

TABLE 3 Propensity functions for the stochastic *lac* operon model

Reaction		Propensity function*†‡
1	$\varnothing \xrightarrow{k_{sMR}} M_R$	$\alpha_1 = V_{E.coli} \cdot N_A \cdot k_{sMR}$
2	$M_R \xrightarrow{k_{sR}} M_R + R$	$\alpha_2 = k_{sR} \cdot M_R$
3	$2R \xrightarrow{k_{2R}} R_2$	$\alpha_3 = \frac{k_{2R}}{V_{E.coli} \cdot N_A} \cdot R \cdot (R-1)$
4	$R_2 \xrightarrow{k_{-2R}} 2R$	$\alpha_4 = k_{-2R} \cdot R_2$
5	$R_2 + O \xrightarrow{k_r} R_2O$	$\alpha_5 = \frac{k_r}{V_{E.coli} \cdot N_A} \cdot R_2 \cdot O$
6	$R_2O \xrightarrow{k_{-r}} R_2 + O$	$\alpha_6 = k_{-r} \cdot R_2O$
7	$2I + R_2 \xrightarrow{k_{dr1}} I_2R_2$	$\alpha_7 = \frac{k_{dr1}}{(V_{E.coli} \cdot N_A)^2} \cdot R_2 \cdot I \cdot (I-1)$
8	$I_2R_2 \xrightarrow{k_{-dr1}} 2I + R_2$	$\alpha_8 = k_{-dr1} \cdot I_2R_2$
9	$2I + R_2O \xrightarrow{k_{dr2}} I_2R_2 + O$	$\alpha_9 = \frac{k_{dr2}}{(V_{E.coli} \cdot N_A)^2} \cdot R_2O \cdot I \cdot (I-1)$
10	$I_2R_2 + O \xrightarrow{k_{-dr2}} 2I + R_2O$	$\alpha_{10} = \frac{k_{-dr2}}{V_{E.coli} \cdot N_A} \cdot I_2R_2 \cdot O$
11	$O \xrightarrow{k_{sMY}} O + M_Y$	$\alpha_{11} = k_{sMY} \cdot O$
12	$M_Y \xrightarrow{k_{1sMY}} M_Y + Y$	$\alpha_{12} = k_{1sMY} \cdot M_Y$
13	$M_Y \xrightarrow{k_{0sMY}} M_Y + Y$	$\alpha_{12} = k_{0sMY} \cdot M_Y$
14	$Y + I_{ex} \xrightarrow{k_p} YI_{ex}$	$\alpha_{13} = k_p \cdot [I_{ex}] \cdot Y$
15	$YI_{ex} \xrightarrow{k_{-p}} Y + I_{ex}$	$\alpha_{14} = k_{-p} \cdot YI_{ex}$
16	$YI_{ex} \xrightarrow{k_{ft}} Y + I$	$\alpha_{15} = k_{ft} \cdot YI_{ex}$
17§	$I_{ex} \xrightarrow{k_t} I$	$\alpha_{16} = V_{E.coli} \cdot N_A \cdot k_t \cdot [I_{ex}]$
18	$I \xrightarrow{k_{-t}} I_{ex}$	$\alpha_{17} = k_t \cdot I$
19	$M_R \xrightarrow{\lambda_{MR}} \varnothing$	$\alpha_{18} = \lambda_{MR} \cdot M_R$
20	$M_Y \xrightarrow{\lambda_{MY}} \varnothing$	$\alpha_{19} = \lambda_{MY} \cdot M_Y$
21	$R \xrightarrow{\lambda_R} \varnothing$	$\alpha_{20} = \lambda_R \cdot R$
22	$R_2 \xrightarrow{\lambda_{R2}} \varnothing$	$\alpha_{21} = \lambda_{R2} \cdot R_2$
23	$Y \xrightarrow{\lambda_Y} \varnothing$	$\alpha_{22} = \lambda_Y \cdot Y$
24	$YI_{ex} \xrightarrow{\lambda_{YIex}} I$	$\alpha_{22} = \lambda_{YIex} \cdot YI_{ex}$
25	$I_2R_2 \xrightarrow{\lambda_{I2R2}} 2I$	$\alpha_{23} = \lambda_{I2R2} \cdot I_2R_2$

*Variables without brackets denote the number of molecules of the corresponding species.
†All propensity functions are in units of min^{-1}.
‡Avogadro's number is $N_A = 6.0221367 \times 10^{14}$ $nmol^{-1}$.
§For the stochastic modeling of I_{ex}-related processes, see Appendix 3.

entitled ''PMF support and memory requirements'' in Supporting Material).

Fig. 6 *a* depicts part of a sample path for the stochastically simulated *lac* operon system and Fig. 6 *b* shows the estimated marginal PMF. A low $[I_{ex}]$ has been used and the PMF appears unimodal, with a heavy tail. On the other hand, for a higher $[I_{ex}]$ (Fig. 6, *c* and *d*), the system exhibits stochastically bistable behavior, since the PMF is bimodal (69). The existence of the heavy tail for low $[I_{ex}]$ and the bistability for higher $[I_{ex}]$ can be attributed to the autocatalytic effect from the action of the LacY permease resulting in the formation of two attracting vicinities. These two vicinities, one for low and one for high $[Y]_T$, are visited with higher probability. Thus, for low $[I_{ex}]$, the system ''wanders'' preferably around the low-attracting vicinity, but also spends some time around the high-attracting vicinity, thereby generating the heavy tail observed in the PMF. For high $[I_{ex}]$, the system spends a significant amount

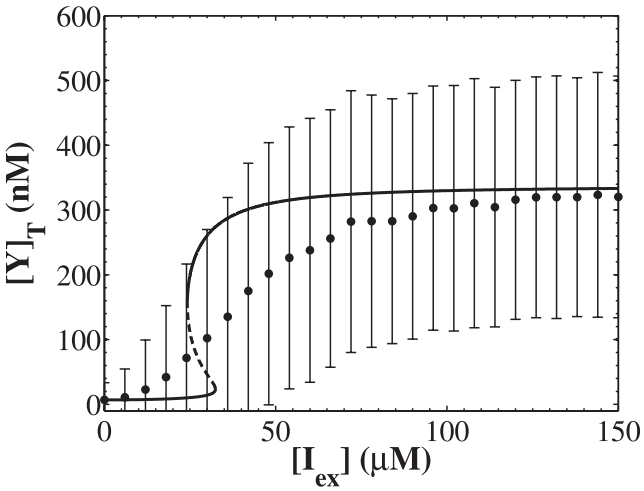

FIGURE 5 Comparison of the stochastic average with the deterministic steady states. The error bars denote two standard deviations (i.e., the minimum and maximum of the error bars correspond to points $\mu \pm \sigma$).

of time around the high-attracting vicinity, and thus, a second mode in the PMF is created.

Bimodality of the PMF signals stochastic bistability; yet one can also detect bistability by analyzing the stationary potential, defined as (70)

$$\varphi^s(x) = -\ln(P^s[X = x]), \tag{14}$$

where $P^s[X = x]$ is the stationary probability that observable X will take the value x. In our case, $X = [Y]_T$ (see Appendix 2 for more information about calculating the PMF. The advantage of using φ^s for our purposes is that it ''magnifies'' minor ''humps'' of the PMF. Note that the maxima of the PMF appear as minima of the potential (attracting wells). Using this tool, we can analyze whether the stochastic model predicts the same bistable regime as the deterministic model. This comparison is of particular interest, since bistability is a key characteristic of the genetic architecture under consideration.

Hence, Fig. 7 *a* portrays the stationary potentials for $[Y]_T$ at various [I] in comparison with the deterministic steady states for the nominal parameter set that dictates slow *lacY* transcription and fast translation. The heavy tails of the PMF correspond to the extended plateaus in the potential. In Fig. 7 *b*, the parameter set of Table 2 was used, whereas the *lacY* transcription constants (k_{s1MY} and k_{s0MY}) have been taken to be 100 times higher and the translation constant (k_{sY}) 100 times lower than the nominal values. Note that their product remains constant, and thus, the deterministic steady states for the three parameter sets differ only in the *lacY* mRNA concentration (see Eqs. S6 and S7). However, the stationary potentials for $[Y]_T$ are vastly different for these three parameter sets. We observe that the combination of fast transcription with slow translation results in well defined modes in the PMF (heavy tails are no longer observed) and a sharper transition through the region of bistability. Furthermore, for this case, the

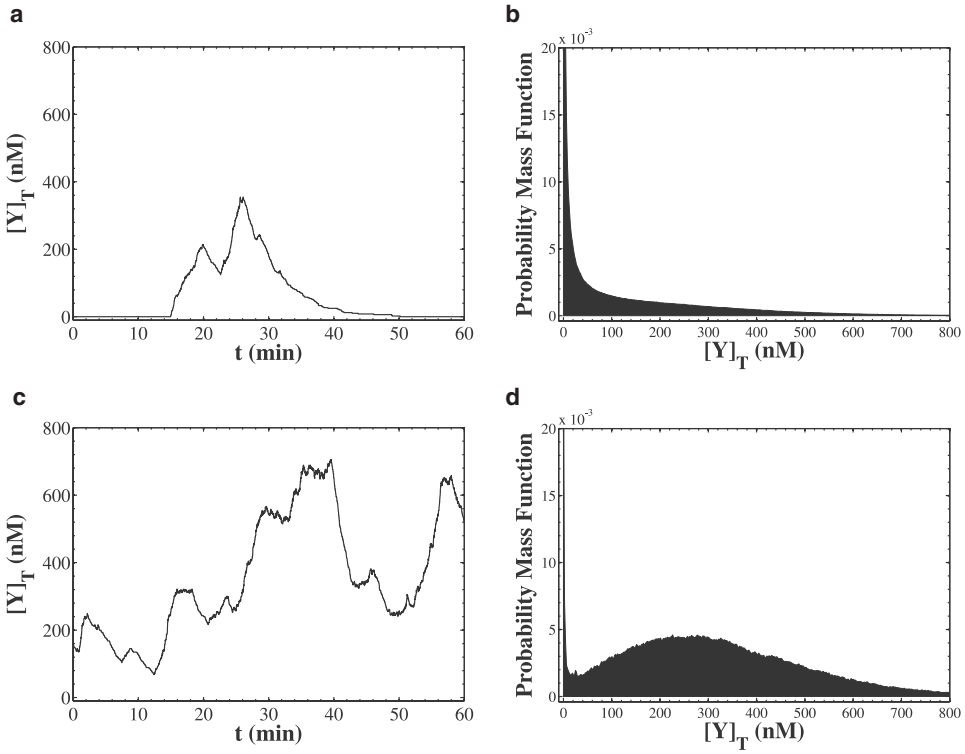

FIGURE 6 Typical sample path for the stochastically simulated *lac* operon system for $[I_{ex}] = 20\ \mu M$ (*a*), and the PMF for this parameter set (*b*). (*c* and *d*) $[I_{ex}] = 100\ \mu M$. Parameters are as in Table 2. Sample histograms for all the species can be found in Figs. S3 and S4.

stochastically bistable regime is shifted closely to the deterministically bistable one.

These observations can be explained by the key role of LacY in the positive feedback mechanism: fast *lacY* transcription but slow translation means that the *lacY* mRNA dynamics will faithfully follow the current state of the operator. Noise in this case is produced at the translational level, but the operator fluctuations between the free and the repressor-bound state are still inherited to the LacY concentration and amplified through the positive feedback loop. However, when *lacY* is transcribed slowly, a small number of *lacY* mRNAs exist on average in the cell. Thus, it is ''more difficult to detect'' whether a change on *lacY* mRNA is due to stochasticity or to a change in the current state of the repressor. This fuzziness is exhibited by the large plateaus in the potential and the destruction of bistability in comparison to the deterministic model's predictions.

Such effects are not observed when the transcriptional and translational rates of only *lacI* are altered, as shown in Fig. 7 *c*, in which k_{sMR} has been taken 100-fold higher and the k_{sR} 100-fold lower. This lack of effect is probably because LacI is not part of the positive feedback mechanism. Yet, if *lacI* and *lacY* transcriptional rates are simultaneously taken to be 100-fold higher (and their translational rates 100-fold lower (Fig. 7 *d*)), one observes potentials that are much sharper than in the case where only *lacY* transcription is fast (Fig. 7 *b*). Moreover, the stochastically bistable regime seems to have shrunk in comparison to the deterministically bistable regime. These effects can be attributed to the negative feedback of LacI to the *lacY* transcription: when *lacI* transcription is slow (and translation fast), the LacI concentration fluctuates stochastically within a large range of values, thereby exerting negative feedback with a strength that varies stochastically. This variation creates a blurring effect in the overall PMF. On the other hand, for fast *lacI* transcription (slow translation), the fluctuations in the LacI concentration are narrowed, and thus, the strength of the negative feedback loop is less variable. As a result, the autocatalytic mechanism can generate a sharp transition through the stochastically bistable regime, and the modes of the PMF appear narrower and well defined.

The aforementioned simulations demonstrated the effect of transcriptional and translational rates of *lacI* and *lacY* on the stationary potential (and the PMF). Yet an integral part of the *lac* operon system is the derepression mechanisms, the rate values of which are expected to affect the stationary potential without necessarily affecting the deterministic bifurcation structure. Thus, Fig. 7, *e* and *f*, shows the stationary potentials for $[Y]_T$ and the deterministic steady states versus IPTG concentrations in the case where only the first derepression mechanism is taken into account (inducer binding to free repressor, reactions vii, viii). For these simulations, fast *lacY* transcription and slow translation was considered, to distinguish the effect of the derepression mechanisms from the blurring and plateaus generated by the low mRNA concentrations.

In Fig. 7 *e*, the binding and unbinding rate constants are taken to be 10-fold lower than those of the nominal case,

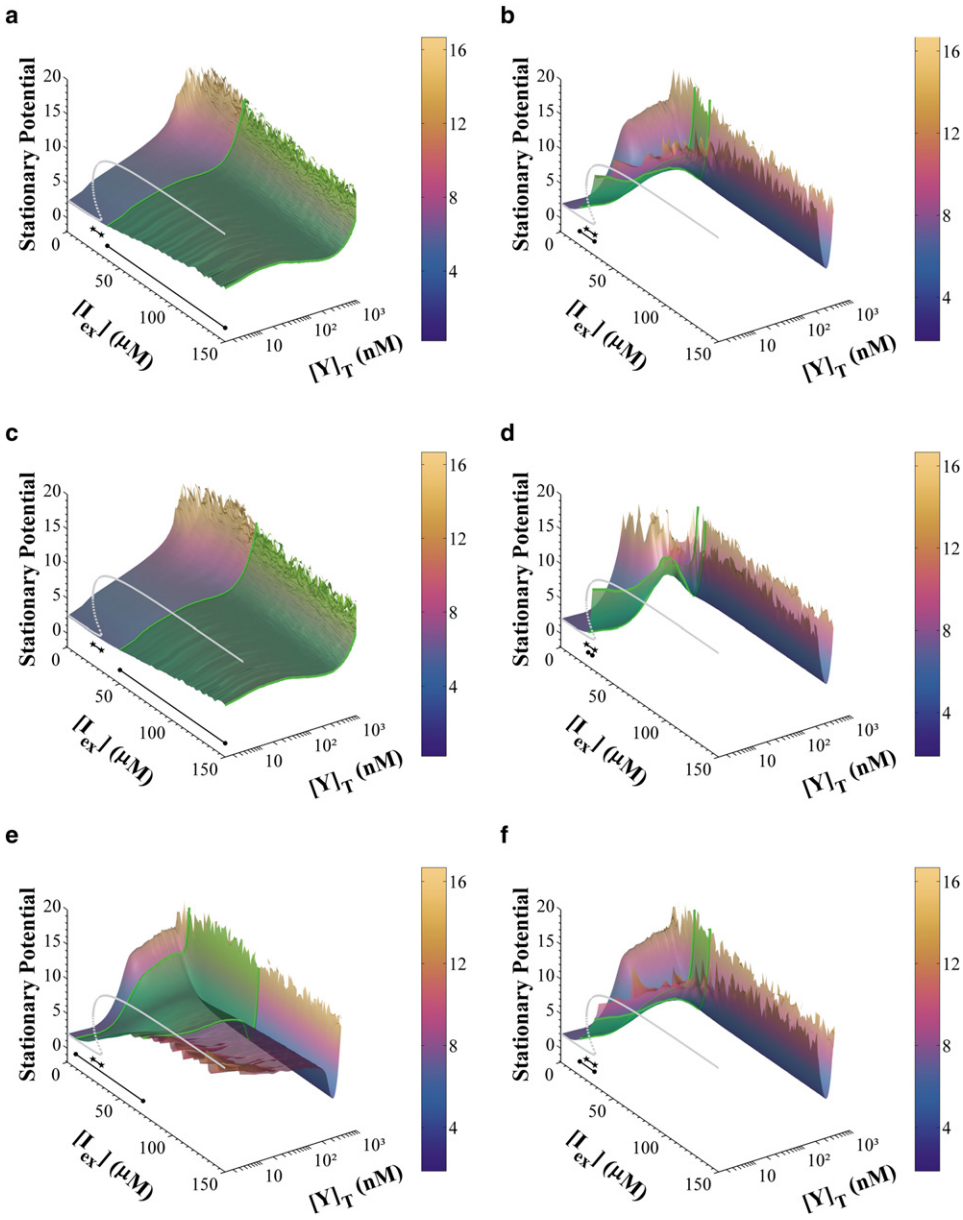

FIGURE 7 The stationary potential for $[Y]_T$ compared to the deterministic bifurcation diagram for a range of IPTG concentrations shows the effect of stochasticity on the behavior of the system in different parameter regimes. (*a*) Nominal parameter set (Table 2). (*b*) 100-fold faster *lacY* transcription ($k_{s1MY} = 50\ min^{-1}$, $k_{s0MY} = 1\ min^{-1}$) and slow translation ($k_{sY} = 0.3\ min^{-1}$). (*c*) 100-fold faster *lacI* transcription ($k_{sMR} = 23\ min^{-1}$) and slow translation ($k_{sR} = 0.15\ min^{-1}$). (*d*) Simultaneous 100-fold faster *lacY* and *lacI* transcription and slow translation for both proteins ($k_{s1MY} = 50\ min^{-1}$, $k_{s0MY} = 1\ min^{-1}$, $k_{sMR} = 23\ min^{-1}$, $k_{sY} = 0.3\ min^{-1}$, $k_{sR} = 0.15\ min^{-1}$). (*e*) 10-fold slower repressor-operator association and dissociation with only the first derepression mechanism, considering fast transcription and slow translation for *lacY* ($k_r = 96\ nM^{-1}\cdot min^{-1}$, $k_{-r} = 0.24\ min^{-1}$, $k_{dr2} = 0\ nM^{-2}\cdot min^{-1}$, $k_{-dr2} = 0\ nM^{-1}\cdot min^{-1}$, $k_{s1MY} = 50\ min^{-1}$, $k_{s1MY} = 1\ min^{-1}$, $k_{sY} = 0.3\ min^{-1}$). (*f*) 10-fold faster repressor-operator association and dissociation with only the first derepression mechanism, considering fast *lacY* transcription and slow translation ($k_r = 9600\ nM^{-1}\cdot min^{-1}$, $k_{-r} = 24\ min^{-1}$, $k_{dr2} = 0\ nM^{-2}\cdot min^{-1}$, $k_{-dr2} = 0\ nM^{-1}\cdot min^{-1}$). The stochastic bistable (bimodal) regime is indicated by ●——● and the deterministic regime by ★——★. Surface color corresponds to stationary potential values and the bimodal regime is shaded green. Parameters are as in Table 2 unless otherwise noted.

whereas in Fig. 7 *f*, those rate constants are taken to be 10-fold higher than the nominal case (also, k_{dr2} and k_{-dr2} are both zero, since only the first derepression mechanism is functional). For both cases, the deterministic bifurcation diagram is the same, since Eq. 6 at steady state gives

$$\frac{k_r}{k_{-r}} = \frac{([O]_T - [O])}{[R_2]\cdot[O]}. \tag{15}$$

and thus, if the binding affinity of the repressor to the operator (k_r/k_{-r}) is kept constant, the asymptotic solution of the deterministic system does not change. However, the stochastic bistable region is drastically affected and apparently does not coincide with that of the deterministic model.

Specifically, Fig. 7 *e* demonstrates that for the stochastic model, slower repressor-operator interaction creates bimodality at an extended [IPTG] region before the left and after the right turning point. This phenomenon could be attributed to the dynamics of protein production being comparable to the repressor binding and unbinding to the operator. Therefore, the protein production machinery senses the stochastic fluctuations of the operator between the free and occupied state, and thus bistability is observed for a wide IPTG range. On the other hand, faster repressor-operator interaction reverts this extension of the bimodal regime. This reversion could be attributed to the time averaging that may occur for fast binding-unbinding dynamics: the protein production depends on the concentration of the free repressor. Thus, if the binding and unbinding is extremely fast, the protein production machinery will merely sense an average free repressor concentration for a wide range of external

IPTG concentrations; consequently, bimodality will be suppressed.

Thus, we clearly see that biomolecular parameters that do not affect the temporal asymptotic behavior of the deterministic model (such as the actual kinetic rates keeping their ratio constant) can have a strong effect on the behavior of the stochastic model. The region of the parameter space for which bistability is observed can be extended or shrunk.

Not all parameters were found to have such pronounced effects though: similar simulations were performed for the case of the second derepression mechanism (inducer binding to the repressor-operator complex, reactions ix, x) by changing the rate values of the repressor-inducer-operator binding and unbinding (k_{dr2} and k_{-dr2} of reactions ix, x to be 100-fold higher or 100-fold lower. However, no appreciable change of the bimodal regime was observed (see Fig. S2, *a* and *b*; note that for this case the deterministic bifurcation diagram changes slightly). Furthermore, we observed only a slight extension of the bimodal regime when taking the repressor-inducer binding and unbinding rates (k_{dr1} and k_{-dr1} of reactions vii, viii) to be 100-fold lower than the nominal values (Fig. S2, *c* and *d*; note that the deterministic bifurcation diagram changes for this case, too). However, this effect was much weaker than that created by slower repressor-operator interaction. This lack of effect can be attributed to the fact that the aforementioned derepression and induction reactions (ix, x and vii, viii respectively) contain a species that exists in very high concentrations, namely the inducer IPTG. Thus, the stochasticity generated by those reactions is negligible in comparison to that generated by the repressor-operator binding and unbinding reactions, in which all participating species have low copy numbers. In view of this observation, we did not perform simulations with different rate constants for the IPTG-facilitated import reactions (xiv–xvi), since they contain species with high copy numbers.

The PMF and the stationary potential presented so far contain information only at the asymptotic level, in the sense that they give the probability of finding $[Y]_T$ at a specific value if we wait long enough. However, the stochastic model exhibits rich behavior also at the temporal level: in the bistable regime, noise-induced transitions between the two attracting vicinities are observed. The frequency of such transitions is quantified by the first passage time (FPT), which is the random time required for a transition from one attracting vicinity to another. The mean FPT (MFPT) is the mean of this random time (43). MFPTs can be thought of as quantifying the relative stability of the two attracting vicinities: the higher the MFPT for a transition from the lower to the upper vicinity, $\overline{T}_{low\to up}$, the more stable the lower vicinity and vice versa. Further, the ratio of the MFPTs, $\overline{T}_{low\to up}/\overline{T}_{up\to low}$, is approximately equal to the ratio of the areas underneath the modes of the stationary PMF, $P^s{}_{low}/P^s{}_{up}$ (71). In our simulations, MFPTs and the standard deviations of FTPs were estimated from single-shot long simulations, typically 10^4–10^6 min, by using the vicinities $Y_T = 5$ molecules and $Y_T = 120$ molecules as reference low and high vicinities.

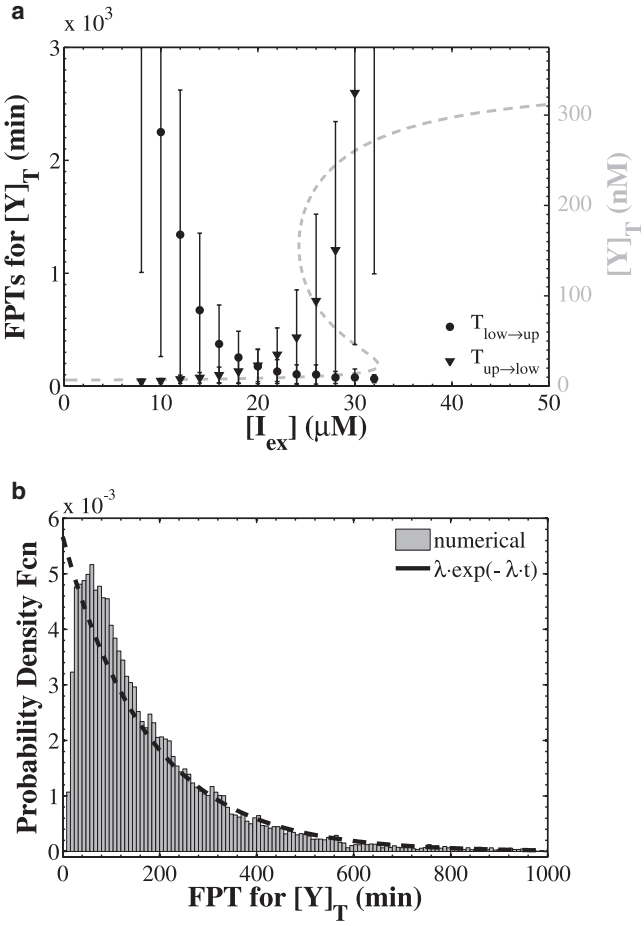

FIGURE 8 (*a*) MFPTs for the transition of $[Y]_T$ from the lower to the upper attracting vicinity (*circles*) or vice versa (*triangles*) for a range of extracellular IPTG concentrations. Fast *lacY* transcription and slow translation were considered. The minimum and maximum of the error bars correspond to the MFPT ± 1 SD. Superimposed for comparison is the corresponding deterministic bifurcation diagram for $[Y]_T$ (secondary *y* axis). (*b*) The probability density function for the FPT $T_{low\to up}$ for $[I_{ex}] = 20\ \mu M$. The MFPT is $1/\lambda \approx 179$ min. Parameters are as in Fig. 7 *b*.

Fig. 8 shows the MFPTs with error bars corresponding to the standard deviations of the FPTs for the case of fast *lacY* transcription and slow translation, in which the transition through the bistable regime is sharp. Circles are used to denote MFPTs for transitions from the lower to the upper attracting vicinities ($\overline{T}_{low\to up}$) and triangles for the opposite transitions ($\overline{T}_{up\to low}$). For low IPTG concentrations, the transitions from the lower to the upper vicinity are extremely rare, and if the system at some point approaches the upper vicinity state, it will rapidly transit toward the lower one. The opposite happens for high IPTG concentrations. Between these extreme cases exists the bistable regime, in which a swapping of the relative magnitudes of the MFPTs $\overline{T}_{low\to up}$ and $\overline{T}_{up\to low}$ occurs.

A more detailed picture of the stochastic dynamics of transitions is given by the distribution of the FPTs (Fig. 8 *b*). In fact, it has been argued that for one-dimensional stochastic systems, the FPT follows an approximately exponential distribution (72,73), $p^{s}(\tau) = \lambda \cdot e^{-\lambda \cdot \tau}$. For multivariate systems with a separation of timescales, the FPT behaves approximately as in the one-dimensional case (72). A statistical analysis of the FPTs for our *lac* operon model indeed shows an agreement between the observed distribution and the theoretically postulated exponential one (Fig. 8 *b*). This agreement also explains the fact that the estimated standard deviations are approximately equal to the value of the mean (Fig. 8 *a*), since for the exponential distribution, both are equal to $1/\lambda$.

We have so far discussed the behavior of the system on two levels: the first pertains to the temporal asymptotic behavior, which was analyzed in terms of the PMF and the stationary potential. The second level pertains to shorter timescales, those of the noise-induced transitions between the attracting vicinities, in the case where the system is stochastically bistable. We are now moving to a third level, in which it is also possible to analyze the much shorter timescales of the inherent noise created by the random occurrence of chemical reaction events. Our main tool for this investigation will be the autocovariance function, defined for observable X as

$$\kappa_X(t_1, t_2) = \langle [X(t_1) - \langle X(t_1) \rangle] \cdot [X(t_2) - \langle X(t_2) \rangle] \rangle. \quad (16)$$

In our case, $X = [Y]_T$. The autocovariance $\kappa_X(t_1, t_2)$ quantifies trends between two points in time and for a wide sense stationary process it is only a function of the time lag; thus, $\kappa_X(t, t + \tau) = \kappa_X(\tau)$. Therefore, it shows the time window for which the system retains its memory. Once we have computed the autocovariance as predicted by our model, we can compare it with the experimental data (74).

Fig. 9 *a* shows that $\kappa_X(\tau)$ decays exponentially faster as τ increases. Thus, the system progressively ''forgets'' its previous history. The autocorrelation time τ_c is indicative of the timescales for which the system still ''remembers'' its history, and was computed from the equation

$$\frac{\kappa_X(\tau_c)}{\kappa_X(0)} = \frac{1}{e}. \quad (17)$$

In Fig. 9 *b*, the autocorrelation time (τ_c) is plotted with respect to the extracellular IPTG concentration. It is clear that τ_c depends on the IPTG concentration, and for the bistable regime, it assumes values significantly larger than those pertaining to the monostable regimes (50 min in the bistable vs. <10 min in the monostable regime). This effect can be attributed to the noise-induced transitions that follow much slower dynamics than the intrinsic noise and thus result in much higher autocorrelation times in the stochastic bistable regime. Indeed, the maximum autocorrelation time ($\tau_{c,max} \approx$ 50 min) occurs for $[I_{ex}] \approx 20\ \mu M$, which is outside of the deterministic bistable region, but it corresponds to the point

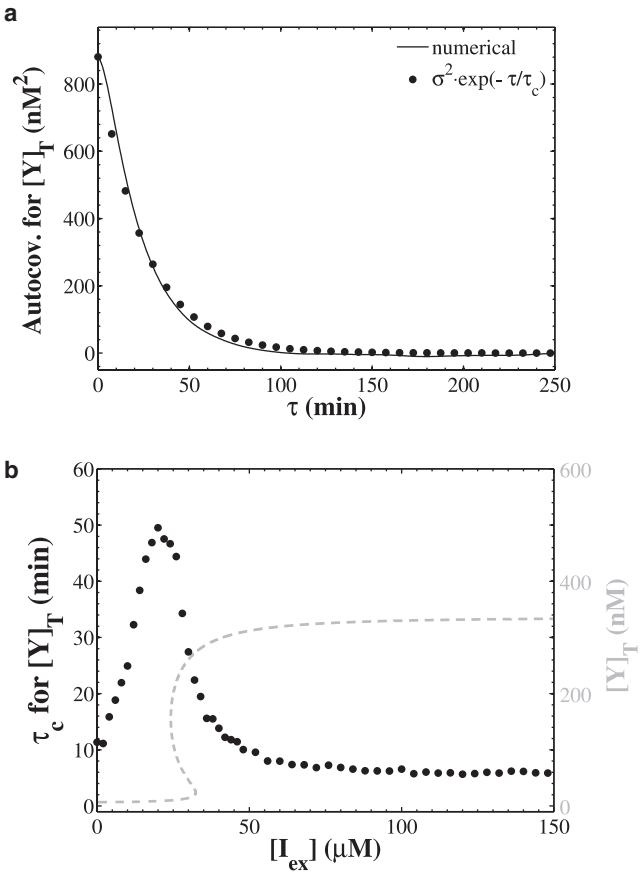

FIGURE 9 (*a*) Autocovariance function for extracellular IPTG concentration $[I_{ex}] = 10\ \mu M$. The autocovariance function decays exponentially fast, with an autocorrelation time of $\tau_c \approx 25$ min in this case. (*b*) Dependence of the autocorrelation times on the induction levels as quantified by $[I_{ex}]$. Superimposed for comparison is the corresponding deterministic bifurcation diagram for $[Y]_T$ (secondary *y* axis). Parameters are as in Fig. 7 *b*.

where the system spends approximately the same mean time in the upper and lower attracting vicinities. The latter fact is revealed by observing Fig. 8 *a*: the graphs for $\overline{T}_{low \to up}$ and $\overline{T}_{up \to low}$ versus $[I_{ex}]$ cross at $[I_{ex}] \approx 20\ \mu M$; therefore, at this point the noise-induced transitions have a maximal contribution to the value of τ_c. However, since these transitions follow much slower dynamics than the intrinsic noise, the autocorrelation time is maximized here. In view of these observations, the assertion by Rosenfeld et al. (74) that intrinsic noise has smaller autocorrelation times than extrinsic noise may not be true for a class of genetic architectures and induction conditions.

SUMMARY

Starting from a network of reactions that incorporates biological information for the *lac* operon genetic switch, we have derived a deterministic model and its corresponding stochastic model for this system.

According to both models, the system exhibits bistability. The deterministic model predicts that certain biomolecular

parameters can greatly affect the extent and positioning of the bistable regime. Specifically, stronger repressor-operator binding, weaker repressor-inducer binding or lower total operator concentrations shift the bistable regime to higher extracellular IPTG concentrations. On the other hand, there are parameter changes that do not affect the steady-state $[Y]_T$ concentration of the deterministic model, but strongly affect the stationary behavior of the stochastic model. Thus, such effects are genuine outcomes of stochasticity. Specifically, faster *lacY* transcription and slower translation rates result in sharper transitions through the stochastically bistable regime and narrower probability distributions. These observations may be explained by the noise generated at the transcriptional level being smaller in the case of fast *lacY* transcription. Thus, the operator fluctuations can be faithfully amplified through the positive feedback loop and produce a clearly bistable behavior.

Moreover, slower repressor-operator binding and unbinding rates result in a broadening of the stochastically bistable region even if the repressor-operator dissociation constant remains the same. Such effects could be attributed to the operator fluctuations being ''inherited'' to the LacY time course in the case where the LacY and *lacO* dynamics have similar timescales. Furthermore, faster LacY production and degradation dynamics have a similar effect of broadening the stochastic bistable regime. Since bistability is a key characteristic of the behavior of the *lac* operon system, it follows that stochasticity can enhance the robustness of the system by extending the bistable region.

The relative stability of the attracting vicinities generated in the stochastic model can be quantified by the FPTs, that is, the random times needed for a jump between the attracting vicinities. The FPTs follow approximately exponential distributions, and their means were found to depend strongly on the extracellular IPTG concentration. For higher inducer concentrations, the upper attracting vicinity is more stable, resulting in lower MFPTs for an upward jump (from the lower to the upper vicinity). Stability is interchanged for lower IPTG concentrations.

Moreover, the stochastic model makes it possible to analyze the statistics of the random fluctuations in the concentrations of LacY at the stationary phase. The autocovariance function was found to decay exponentially, with autocorrelation times highly dependent on the induction level as quantified by the extracellular IPTG concentration. Therefore, in the monostable regimes these times were significantly smaller than those observed in the bistable regime, an effect that can be attributed to the noise-induced transitions.

In conclusion, we have presented a comparative analysis of correspondent deterministic and stochastic models for the *lac* operon system. The incorporation of biological information into the models revealed the effect of biomolecular parameters in the presence and absence of stochasticity. These parameters can be modulated experimentally, and thus the presented models can provide valuable insight into the underlying biological processes. More important, the comparison of the predications of the two models makes possible the isolation of the genuine effects of stochasticity on key characteristics of *lac* operon behavior, such as the extent of the bistable regime and thus the robustness of the system.

APPENDIX 1: ORIGINS OF EQUATION 1

Equation 1 essentially originates from Hess's law for the Gibbs free energy applied to the set of chemical equilibria v–x. Hess's law expresses the conservation of energy, denoted as state function ΔG, regardless of the path through which it is to be determined. In our case, there exist three linearly dependent chemical equilibria:

$$R_2 + O \overset{K_1}{\rightleftarrows} R_2O \qquad \text{(v, vi)}$$

$$2I + R_2 \overset{K_2}{\rightleftarrows} I_2R_2 \qquad \text{(vii, viii)}$$

$$2I + R_2O \overset{K_3}{\rightleftarrows} I_2R_2 + O, \qquad \text{(ix, x)}$$

where K_i denotes the equilibrium constant of reversible reaction 1. Linear dependence in the equilibria means that there are two ''paths'' for going from one state to another:

$$\text{path 1} : R_2 + O + 2I \overset{\text{fwd 1}}{\rightarrow} R_2O + 2I \overset{\text{fwd 3}}{\rightarrow} I_2R_2 + O \quad \text{(A1)}$$

$$\text{path 2} : R_2 + O + 2I \overset{\text{fwd 2}}{\rightarrow} R_2I_2 + O \quad \text{(A2)}$$

where fwd (bwd) i means that reversible reaction 1 is taking place in the forward (backward) direction. Since the initial and final states for both paths are the same, it follows that the Gibbs free energy for the three equilibria satisfies the equation

$$\begin{aligned} &\Delta G_1 + \Delta G_3 = \Delta G_2 \Rightarrow \\ &R\cdot T\cdot \ln(K_1) + R\cdot T\cdot \ln(K_3) = R\cdot T\cdot \ln(K_2) \Rightarrow \\ &K_1\cdot K_3 = K_2 \end{aligned} \quad \text{(A3)}$$

The latter equation is essentially Eq. 1.

APPENDIX 2: MONTE CARLO SIMULATIONS AND CALCULATION OF STATISTICS

Kinetic Monte Carlo simulations were performed using the direct method of Gillespie's algorithm. Due to the ergodic properties of the process under consideration, sampling over the ensemble is equivalent to sampling over time (43 (pp. 190–191)). Thus, long simulations (10^4–10^6 min) were performed and samples were taken over constant Δt. Subsequently, the statistical properties of interest were estimated from these samples.

Thus, for calculation of the marginal PMF for species X, Δt was taken as 5×10^{-2} min and the following estimator was used:

$$\widehat{p}_X(j) = \frac{1}{N}\cdot \sum_{i=1}^{N} \mathbf{1}_{\{X_i = j\}} \quad \text{(A4)}$$

where $p_X(j)$ is the probability of observing j molecules of species X ($j = 0, 1, \ldots$), N is the number of samples, and $\mathbf{1}_{\{E\}}$ is an indicator that takes a value of 1 if event E is true and 0 otherwise. The probabilities p_j were subsequently used in the calculation of the mean μ_X and variance $\sigma_X{}^2$ of the number of molecules of X. If j_{max} denotes the maximum number of molecules of X within our samples, then

$$\hat{\mu}_X = \sum_{j=0}^{j_{\max}} p_j \cdot j \tag{A5}$$

$$\hat{\sigma}_X = \sum_{j=1}^{j_{\max}} p_j \cdot (j - \mu_X)^2. \tag{A6}$$

The autocovariance function $\kappa(\tau)$ can be calculated at time lags, τ, that are integer multiples of the Δt used in the sampling of the stochastic path that was taken at $\Delta t = 5 \times 10^{-1}$ min. The estimator that was used is

$$\hat{\kappa}_X(k \cdot \Delta t) = \frac{1}{N-k-1} \cdot \left\{ \sum_{i=1}^{N} \mathrm{X}_i \cdot \mathrm{X}_{i-k} - \frac{1}{N-k} \cdot \sum_{i=1}^{N} \mathrm{X}_i \cdot \sum_{i=1}^{N} \mathrm{X}_{i-k} \right\}. \tag{A7}$$

Note that the above estimators for the mean variance and autocovariance refer to the numbers of molecules of species X. In the comparisons with the deterministic model, we need to work with concentrations because the deterministic results are expressed in concentrations. For example we need to calculate $\hat{\mu}_{[X]}$, the mean concentration of species X. Thus, since

$$[\mathrm{X}] = \frac{\mathrm{X}}{N_\mathrm{A} \cdot V_{\mathrm{E.coli}}} \tag{A8}$$

it follows that

$$\hat{\mu}_{[\mathrm{X}]} = \frac{\hat{\mu}_\mathrm{X}}{N_\mathrm{A} \cdot V_{\mathrm{E.coli}}} \tag{A9}$$

$$\hat{\sigma}_{[\mathrm{X}]} = \frac{\hat{\sigma}_\mathrm{X}}{(N_\mathrm{A} \cdot V_{\mathrm{E.coli}})^2} \tag{A10}$$

$$\hat{\kappa}_{[\mathrm{X}]}(k \cdot \Delta t) = \frac{\hat{\kappa}_\mathrm{X}(k \cdot \Delta t)}{(N_\mathrm{A} \cdot V_{\mathrm{E.coli}})^2}. \tag{A11}$$

For the calculation of the FPTs, the following methodology was developed: first, two reference states were defined, the high state, e.g., for species X having a copy number of 350, and the low state, for X = 5. During the simulation or in postprocessing mode, the time instances for which the system exists in the low and high reference states are stored ordered in two separate vectors, t_{low} and t_{high} (these time instances are multiples of a time step, Δt, taken as 10^{-2} min). Then, to find the distribution of the FPT from the low to the high reference state, samples were obtained as follows. Let $t_{\mathrm{low}[i]}$ be an element of vector t_{low}. The code locates the first element $t_{\mathrm{high}[j]}$ that satisfies $t_{\mathrm{high}[j]} > t_{\mathrm{low}[i]}$. Thus, $(t_{\mathrm{high}[j]} - t_{\mathrm{low}[i]})$ is one sample. Subsequent samples are taken for different i values (by scanning vector t_{low}). Using the same methodology, the FPT from the high to the low reference state can also be computed. The MFPT is estimated as the average of the obtained samples and the variance as the sample variance.

For more information on the initial conditions used, the sample sizes, and the filtering of the transient parts of the simulations, see "ICs, sample sizes, and filtering of transient part" in Supporting Material.

APPENDIX 3: DERIVATION OF THE PROPENSITIES FOR $\mathrm{I_{EX}}$-RELATED PROCESSES

Consider a cell of volume V and membrane area A (where A and V are both constant). The extracellular IPTG molecules that continuously "hit" the membrane of the cell can either be absorbed into the intracellular space or bounce back without leaving the extracellular space. Let us first deal with free IPTG diffusion through the membrane. We approximate the cell membrane with a planar surface at small spatial scales (essentially we are dealing with a differential area δA of the membrane). We also approximate the IPTG molecule with a sphere. Then, an IPTG molecule will hit the membrane if the distance between the center of the molecule and the surface reduces to half the diameter of the IPTG molecule $d_{\mathrm{IPTG}}/2$. Thus, the differential area is covered by a "collision volume" (Fig. 10):

$$\delta V_{\mathrm{coll}} = \delta A \cdot (-\underset{\sim}{u}_{\mathrm{IPTG}}, \underset{\sim}{n}_{\mathrm{A}}) \cdot 1_{\{(-\underset{\sim}{u}_{\mathrm{IPTG}}, \underset{\sim}{n}_{\mathrm{A}})>0\}} \cdot \delta t, \tag{A12}$$

where $\mathbf{1}_{\{\mathrm{E}\}}$ is unity when E is true and zero otherwise (the corresponding term in Eq. A12 is unity only when the molecule approaches the membrane); u_{IPTG} is the velocity of the IPTG molecule relative to the membrane and $\underset{\sim}{n}_A$ is the normalized vector perpendicular to the membrane surface with direction toward the outer part of the cell. (x, y) denotes the dot product of vectors x and y. Thus, if the IPTG molecule is inside the collision volume, it will hit the membrane at the next δt time interval. Since IPTG molecules are uniformly distributed in the extracellular space, it follows that the average probability of one IPTG molecule hitting the membrane is

$$\left\langle \frac{\delta V_{\mathrm{coll}}}{V_{\mathrm{ex}}} \right\rangle = A \cdot u_{\mathrm{m}} \cdot \frac{\delta t}{V_{\mathrm{ex}}}, \tag{A13}$$

where A is the surface area of the whole membrane and u_{m} is the mean velocity at which IPTG molecules approach the membrane, defined as

$$u_{\mathrm{m}} = \int\int (-\underset{\sim}{v}, \underset{\sim}{n}_{\mathrm{A}}) \cdot \mathbf{1}_{\{(-\underset{\sim}{u}_{\mathrm{IPTG}}, \underset{\sim}{n}_{\mathrm{A}})>0\}} \cdot p_{\underset{\sim}{u}_{\mathrm{IPTG}}}(\underset{\sim}{v}) d\underset{\sim}{v}\, dA. \tag{A14}$$

If the number of IPTG molecules per unit time that hit the membrane is high, let f_t denote the probability of a successful pass-through given that a hit has occurred.

$$A \cdot u_{\mathrm{m}} \cdot f_{\mathrm{t}} \cdot \frac{\delta \mathrm{t}}{V_{\mathrm{ex}}} = \text{average probability,} \tag{A15}$$

to the first order in δt, that a specific IPTG molecule will successfully pass through the membrane in the next time interval dt.

Furthermore, there exist $\mathrm{I_{ex}}$ molecules uniformly distributed in the extracellular space:

$$\mathrm{I_{ex}} = V_{\mathrm{ex}} \cdot [\mathrm{I_{ex}}] \cdot N_\mathrm{A}, \tag{A16}$$

where $\mathrm{I_{ex}}$ denotes the number of molecules, $[\mathrm{I_{ex}}]$ the concentrations, V_{ex} the extracellular volume, and N_A Avogadro's number. Thus, if we consider the passing-through of one IPTG molecule as a reaction occurring in the intracellular space that leads to the production of one IPTG molecule therein

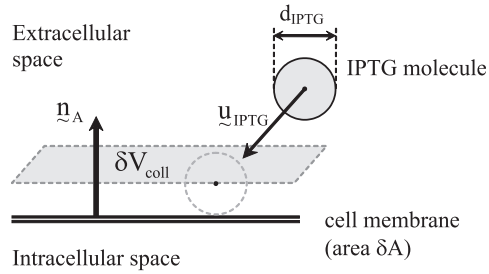

FIGURE 10 An IPTG molecule approaching the membrane of the cell. Collision will occur in the next δt time interval if the molecule is moving toward the membrane and the center of the molecule is inside $\delta V_{\mathrm{coll}} = \delta A \cdot (-\underset{\sim}{u}_{\mathrm{IPTG}}, \underset{\sim}{n}_{\mathrm{A}}) \cdot \delta t$. See text for details.

(assuming that the intracellular space is well stirred), then the average reaction rate (in units of molecules produced per time) will be $c_t^{'}\cdot\langle \mathrm{I_{ex}}\rangle\cdot\delta \mathrm{t}$, where the stochastic reaction constant (having units of inverse time) is

$$c_{\mathrm{t}}^{'} = \frac{A\cdot u_{\mathrm{m}}\cdot f_{\mathrm{t}}}{V_{\mathrm{ex}}}. \tag{A17}$$

Note that $c_t^{'}$ is inversely proportional to the extracellular volume. This is expected: for a fixed amount of molecules in the extracellular space, the average number of molecules that pass through the membrane will be higher if the extracellular space is smaller. Now, the deterministic "reaction rate constant equivalent", k_t, is conventionally defined to be the average stochastic reaction rate (in molecules/time) per unit intracellular volume, V, divided by the average concentration of the "reactant" (namely, the IPTG in the extracellular space):

$$k_{\mathrm{t}} = \frac{1}{V\cdot N_{\mathrm{A}}}\frac{c_{\mathrm{t}}^{'}\cdot\langle[\mathrm{I_{ex}}]\rangle\cdot V_{\mathrm{ex}}\cdot N_{\mathrm{A}}}{\langle[\mathrm{I_{ex}}]\rangle}\Rightarrow k_{\mathrm{t}}\cdot\frac{V}{V_{\mathrm{ex}}} = c_{\mathrm{t}}^{'}. \tag{A18}$$

For our study, we consider the limiting case where the extracellular volume tends to infinity and thus $c_t^{'}$ tends to zero. Further, since the IPTG concentration (intensive quantity) remains constant, the number of IPTG molecules in the extracellular volume also tends to infinity, but the product $c_{\mathrm{t}}^{'}\cdot\langle \mathrm{I_{ex}}\rangle = A\cdot u_{\mathrm{m}}\cdot f_{\mathrm{t}}\cdot\langle[\mathrm{I_{ex}}]\rangle\cdot N_{\mathrm{A}}$ remains constant. In the bulk, there is no distinction between $\langle[\mathrm{I_{ex}}]\rangle$ and $[\mathrm{I_{ex}}]$, and thus we define the following stochastic reaction constant:

$$c_{\mathrm{t}} = c_{\mathrm{t}}^{'}\cdot\langle \mathrm{I_{ex}}\rangle = k_{\mathrm{t}}\cdot\frac{V}{V_{\mathrm{ex}}}\cdot\langle \mathrm{I_{ex}}\rangle = k_{\mathrm{t}}\cdot V\cdot N_{\mathrm{A}}\cdot[\mathrm{I_{ex}}], \tag{A19}$$

which is precisely what was used for the reaction describing the transport of extracellular IPTG into the intracellular space. The derivation of the stochastic kinetic constant for the opposite transport (intracellular IPTG out to the intracellular space) follows from the above.

Finally, for the case of the facilitated IPTG transport, one will have to take into account that the LacY permeases are uniformly distributed on the membrane of the cell covering a fraction ϕ_{Y} of the total membrane area; thus, the collision volume will be

$$\delta V_{\mathrm{coll}} = \delta A\times\phi_{\mathrm{Y}}\cdot\left(-\underset{\sim}{u}_{\mathrm{IPTG}},\underset{\sim}{n}_{\mathrm{A}}\right)\cdot\mathbf{1}_{\{(-\underset{\sim}{u}_{\mathrm{IPTG}},\underset{\sim}{n}_{\mathrm{A}})>0\}}\cdot\delta \mathrm{t}. \tag{A20}$$

ϕ_{Y} can be mapped to the number of the LacY permeases existing in the cell, and this is how the propensity function $k_{\mathrm{p}}\cdot[\mathrm{I_{ex}}]\cdot \mathrm{Y}$ is constructed.

SUPPORTING MATERIAL

Additional figures and equations are available at http://www.biophysj.org/biophysj/supplemental/S0006-3495(08)00100-8.

The authors thank Dr. Kathy Mathhews, Dr. Hongli Zhan (Department of Biochemistry and Cell Biology, Rice University), and Dr. Liskin Swint-Kruse (Department of Biochemistry and Molecular Biology, University of Kansas) for valuable insights on the physiology of the *lac* operon network. We also thank the reviewers for their constructive criticism and their contribution to the improvement of this work. M.S. especially thanks his colleague Konstantinos Spetsieris (Chemical and Biomolecular Engineering, Rice University) for many stimulating discussions regarding this work.

This work was supported in part by the Rice Computational Research Cluster, funded by the National Science Foundation under grant CNS-0421109, and a partnership between Rice University, Advanced Micro Devices, and Cray. Financial support from the National Institutes of Health/National Institute of General Medical Sciences (R01GM071888) is also gratefully acknowledged.

REFERENCES

1. Jacob, F., D. Perrin, C. Sanchez, and J. Monod. 1960. L'operon: groupe de gènes à expression coordonnée par un opérateur. *Comptes Rendus Hebdomadaires des Séances de L'Académie des Sciences. Serie D: Sciences naturelles*. 250:1727–1729.
2. Müller-Hill, B. 1996. The *lac* Operon: A Short History of a Genetic Paradigm. de Gruyter, Berlin.
3. Friedman, A. M., T. O. Fischmann, and T. A. Steitz. 1995. Crystal structure of *lac* repressor core tetramer and its implications for DNA looping. *Science*. 268:1721–1727.
4. Matthews, K. S. 1992. DNA looping. *Microbiol. Mol. Biol. Rev.* 56:123–136.
5. Oehler, S., E. R. Eismann, H. Krämer, and B. Müller-Hill. 1990. The three operators of the *lac* operon cooperate in repression. *EMBO J.* 9:973–979.
6. Lewis, M., G. Chang, N. C. Horton, M. A. Kercher, H. C. Pace, et al. 1996. Crystal structure of the lactose operon repressor and its complexes with DNA and inducer. *Science*. 271:1247–1254.
7. Vilar, J. M., and L. Saiz. 2005. DNA looping in gene regulation: from the assembly of macromolecular complexes to the control of transcriptional noise. *Curr. Opin. Genet. Dev.* 15:136–144.
8. Malan, T. P., A. Kolb, H. Buc, and W. R. McClure. 1984. Mechanism of CRP-cAMP activation of *lac* operon transcription initiation activation of the P1 promoter. *J. Mol. Biol.* 180:881–909.
9. Novick, A., and M. Weiner. 1957. Enzyme induction as an all-or-none phenomenon. *Proc. Natl. Acad. Sci. USA*. 43:553–566.
10. Reznikoff, W. S., and J. N. Abelson. 1978. The *lac* promoter. *In* The Operon. J. H. Miller and W. S. Reznikoff, editors. Cold Spring Harbor Laboratory, Cold Spring Harbor, NY. 221–243.
11. Calos, M. P., and J. H. Miller. 1980. DNA sequence alteration resulting from a mutation impairing promoter function in the *lac* repressor gene. *Mol. Gen. Genet.* 178:225–227.
12. Calos, M. P. 1978. DNA sequence for a low-level promoter of the *lac* repressor gene and an "up" promoter mutation. *Nature*. 274: 762–765.
13. Swint-Kruse, L., H. Zhan, B. M. Fairbanks, A. Maheshwari, and K. S. Matthews. 2003. Perturbation from a distance: mutations that alter LacI function through long-range effects. *Biochemistry*. 42:14004–14016.
14. Suckow, J., P. Markiewicz, L. G. Kleina, J. Miller, B. Kisters-Woike, et al. 1996. Genetic studies of the Lac repressor XV: 4000 single amino acid substitutions and analysis of the resulting phenotypes on the basis of the protein structure. *J. Mol. Biol.* 261:509–523.
15. Markiewicz, P., L. G. Kleina, C. Cruz, S. Ehret, and J. H. Miller. 1994. Genetic studies of the *lac* repressor. XIV. Analysis of 4000 altered *Escherichia coli lac* repressors reveals essential and non-essential residues, as well as "spacers" which do not require a specific sequence. *J. Mol. Biol.* 240:421–433.
16. Falcon, C. M., and K. S. Matthews. 1999. Glycine insertion in the hinge region of lactose repressor protein alters DNA binding. *J. Biol. Chem.* 274:30849–30857.
17. Padan, E., H. K. Sarkar, P. V. Viitanen, M. S. Poonian, and H. R. Kaback. 1985. Site-specific mutagenesis of histidine residues in the *lac* permease of *Escherichia coli*. *Proc. Natl. Acad. Sci. USA*. 82:6765–6768.
18. Griffith, J. S. 1968. Mathematics of cellular control processes II. Positive feedback to one gene. *J. Theor. Biol.* 20:209–216.
19. Yagil, G., and E. Yagil. 1971. On the relation between effector concentration and the rate of induced enzyme synthesis. *Biophys. J.* 11:11–27.
20. Van Dedem, G., and M. Moo-Young. 1973. Cell growth and extracellular enzyme synthesis in fermentations. *Biotechnol. Bioeng.* 15:419–439.
21. Imanaka, T., and S. Aiba. 1977. A kinetic model of catabolite repression in the dual control mechanism in microorganisms. *Biotechnol. Bioeng.* 19:757–764.

22. Toda, K. 1976. Dual control of invertase Biosynthesis in chemostat culture. *Biotechnol. Bioeng.* 18:1117–1124.
23. Gondo, S., K. Venkatasubramanian, W. R. Vieth, and A. Constantinides. 1978. Modeling the role of cyclic AMP in catabolite repression of inducible enzyme biosynthesis in microbial cells. *Biotechnol. Bioeng.* 20:1797–1815.
24. Vieth, W. R., K. Kaushik, and K. Venkatasubramanian. 1982. Role of active transport of inducer in enzyme biosynthesis and process scale-up. *In* Enzyme Engineering: Proceedings of the International Enzyme Engineering Conference. I. Chibata, S. Fukui, and B. Wingard, editors. Plenum Press, London. 45–59.
25. Lee, S. B., and J. E. Bailey. 1984. Genetically structured models for *lac* promoter-operator function in the *Escherichia coli* chromosome and in multicopy plasmids: *Lac* operator function. *Biotechnol. Bioeng.* 26:1372–1382.
26. Lee, S. B., and J. E. Bailey. 1984. Genetically structured models for *lac* promoter-operator function in the chromosome and in multicopy plasmids: *Lac* promoter function. *Biotechnol. Bioeng.* 26:1383–1389.
27. Laffend, L., and M. L. Shuler. 1994. Ribosomal protein limitations in *Escherichia coli* under conditions of high translational activity. *Biotechnol. Bioeng.* 43:388–398.
28. Laffend, L., and M. L. Shuler. 1994. Structured model of genetic control via the *lac* promoter in *Escherichia coli*. *Biotechnol. Bioeng.* 43:399–410.
29. Laffend, L. A. 1991. Production and Secretion of a Recombinant Protein under Control of the *lac* Promoter/Operator in *Escherichia coli*. Cornell University Press, Ithaca, NY.
30. Ray, N. G., W. R. Vieth, and K. Venkatasubramanian. 1987. Regulation of *lac* operon expression in mixed sugar chemostat cultures. *Biotechnol. Bioeng.* 29:1003–1014.
31. Chung, J. D., and G. Stephanopoulos. 1996. On physiological multiplicity and population heterogeneity of biological systems. *Chem. Eng. Sci.* 51:1509–1521.
32. Straight, J. V., and D. Ramkrishna. 1991. Complex growth dynamics in batch cultures: experiments and cybernetic models. *Biotechnol. Bioeng.* 37:895–909.
33. Ramakrishna, R., D. Ramkrishna, and A. E. Konopka. 1996. Cybernetic modeling of growth in mixed, substitutable substrate environments: preferential and simultaneous utilization. *Biotechnol. Bioeng.* 52:141–151.
34. Wong, P., S. Gladney, and J. D. Keasling. 1997. Mathematical model of the *lac* operon: inducer exclusion, catabolite repression, and diauxic growth on glucose and lactose. *Biotechnol. Prog.* 13:132–143.
35. Tian, T., and K. Burrage. 2005. A Mathematical Model for Genetic Regulation of the Lactose Operon. Springer, Berlin/Heidelberg. 1245–1253.
36. Maffahy, J. M., and E. Savev. 1999. Stability analysis for a mathematical model of the *lac* operon. *Q. Appl. Math.* 57:37–53.
37. Yildirim, N., and M. C. Mackey. 2003. Feedback regulation in the lactose operon: a mathematical modeling study and comparison with experimental data. *Biophys. J.* 84:2841–2851.
38. Tanaka, R. J., H. Okano, and H. Kimura. 2006. Mathematical description of gene regulatory units. *Biophys. J.* 91:1235–1247.
39. Carrier, T. A., and J. D. Keasling. 1997. Mechanistic modeling of prokaryotic mRNA decay. *J. Theor. Biol.* 189:195–209.
40. Carrier, T. A., and J. D. Keasling. 1999. Investigating autocatalytic gene expression systems through mechanistic modeling. *J. Theor. Biol.* 201:25–36.
41. Mettetal, J. T., D. Muzzey, J. M. Pedraza, E. M. Ozbudak, and A. van Oudenaarden. 2006. Predicting stochastic gene expression dynamics in single cells. *Proc. Natl. Acad. Sci. USA.* 103:7304–7309.
42. Ozbudak, E. M., M. Thattai, H. N. Lim, B. I. Shraiman, and A. v. Oudenaarden. 2004. Multistability in the lactose utilization network of *Escherichia coli*. *Nature*. 427:737–740.
43. van Kampen, N. G. 1992. Stochastic Processes in Physics and Chemistry. North Holland Personal Library, New York, Amsterdam.
44. Vilar, J. M. G., C. C. Guet, and S. Leibler. 2003. Modeling network dynamics: the *lac* operon, a case study. *J. Cell Biol.* 161:471–476.
45. McAdams, H. H., and A. Arkin. 1997. Stochastic mechanisms in gene expression. *Proc. Natl. Acad. Sci. USA.* 94:814–819.
46. McAdams, H. H., and A. Arkin. 1998. Simulation of prokaryotic genetic circuits. *Annu. Rev. Biophys. Biomol. Struct.* 27:199–224.
47. Kærn, M., T. C. Elston, W. J. Blake, and J. J. Collins. 2005. Stochasticity in gene expression: from theories to phenotypes. *Nat. Rev. Genet.* 6:451–464.
48. Arkin, A., J. Ross, and H. H. McAdams. 1998. Stochastic kinetic analysis of developmental pathway bifurcation in phage l-infected *Escherichia coli* cells. *Genetics.* 149:1633–1648.
49. Hasty, J., J. Pradines, M. Dolnik, and J. J. Collins. 2000. Noise-based switches and amplifiers for gene expression. *Proc. Natl. Acad. Sci. USA.* 97:2075–2080.
50. Samoilov, M., S. Plyasunov, and A. P. Arkin. 2005. Stochastic amplification and signaling in enzymatic futile cycles through noise-induced bistability with oscillations. *Proc. Natl. Acad. Sci. USA.* 102:2310–2315.
51. Kepler, T. B., and T. C. Elston. 2001. Stochasticity in transcriptional regulation: origins, consequences, and mathematical representations. *Biophys. J.* 81:3116–3136.
52. Gillespie, D. T. 1977. Exact stochastic simulation of coupled chemical reactions. *J. Phys. Chem.* 81:2340–2361.
53. Schmitz, A., U. Schmeissner, and J. H. Miller. 1976. Mutations affecting the quaternary structure of the *lac* repressor. *J. Biol. Chem.* 251:3359–3366.
54. Oehler, S., M. Amouyal, P. Kolkhof, B. von Wilcken-Bergmann, and B. Muller-Hill. 1994. Quality and position of the three *lac* operators of *E. coli* define efficiency of repression. *EMBO J.* 13:3384–3385.
55. Chen, J., R. Surendran, J. C. Lee, and K. S. Matthews. 1994. Construction of a dimeric repressor: dissection of subunit interfaces in Lac repressor. *Biochemistry.* 33:1234–1241.
56. Chen, J., and K. S. Matthews. 1992. Deletion of lactose repressor carboxyl-terminal domain affects tetramer formation. *J. Biol. Chem.* 267:13843–13850.
57. Ohshima, Y., T. Mizokoshi, and T. Horiuchi. 1974. Binding of an inducer to the *lac* repressor. *J. Mol. Biol.* 89:127–136.
58. Bell, C. E., and M. Lewis. 2000. A closer view of the conformation of the Lac repressor bound to operator. *Nat. Struct. Biol.* 7:209–214.
59. O'Gorman, R. B., J. M. Rosenberg, O. B. Kallai, R. E. Dickerson, K. Itakura, et al. 1980. Equilibrium binding of inducer to *lac* repressor-operator DNA complex. *J. Biol. Chem.* 255:10107–10114.
60. Chen, J., S. Alberti, and K. S. Matthews. 1994. Wild-type operator binding and altered cooperativity for inducer binding of *lac* repressor dimer mutant R3. *J. Biol. Chem.* 269:12482–12487.
61. Narang, A. 2007. Effect of DNA looping on the induction kinetics of the lac operon. *J. Theor. Biol.* 247:695–712.
62. Kepes, A. 1960. Kinetic studies on the galactoside-permease in *E. coli*. *Biochim. Biophys. Acta.* 40:70–84.
63. Cohn, M., and K. Horibata. 1959. Analysis of the differentiation and of the heterogeneity within a population of *Escherichia coli* undergoing induced β-galactosidase synthesis. *J. Bacteriol.* 78:613–623.
64. Salinger, A. G., N. M. Bou-Rabee, R. P. Pawlowski, E. D. Wilkes, E. A. Burroughs, et al. 2002. LOCA 1.0 Library of Continuation Algorithms: Theory and Implementation Manual. Sandia National Laboratories, Albuquerque, NM.
65. Gilbert, W., and B. Müller-Hill. 1966. Isolation of the Lac repressor. *Proc. Natl. Acad. Sci. USA.* 56:1891–1898.
66. Müller-Hill, B., L. Crapo, and W. Gilbert. 1968. Mutants that make more *lac* repressor. *Proc. Natl. Acad. Sci. USA.* 59:1259–1264.
67. McQuarrie, D. A. 1967. Stochastic approach to chemical kinetics. *J. Appl. Probab.* 4:413–478.

68. Gillespie, D. T. 1976. A general method for numerically simulating the stochastic time evolution of coupled chemical reactions. *J. Comput. Phys.* 22:403–434.

69. Horsthemke, W., and R. Lefever. 1983. Noise-Induced Transitions. Springer-Verlag, New York.

70. Gillespie, D. T. 1979. A pedestrian approach to transitions and fluctuations in simple nonequilibrium chemical systems. *Physica A.* 95:69–103.

71. Gillespie, D. T. 1981. On the calculation of mean first passage times for simple random walks. *J. Chem. Phys.* 74:5295–5299.

72. Procaccia, I., and J. Ross. 1977. Stability and relative stability in reactive systems far from equilibrium. II. Kinetic analysis of relative stability of multiple stationary states. *J. Chem. Phys.* 67:5565–5571.

73. Gillespie, D. T. 1980. Transition time statistics in simple bi-stable chemical systems. *Physica A.* 101:535–551.

74. Rosenfeld, N., J. W. Young, U. Alon, P. S. Swain, and M. B. Elowitz. 2005. Gene regulation at the single-cell level. *Science.* 307:1962–1965.

75. Santillán, M., and M. C. Mackey. 2004. Influence of catabolite repression and inducer exclusion on the bistable behavior of the *lac* operon. *Biophys. J.* 86:1282–1292.

76. Goeddel, D. V., D. G. Yansura, and M. H. Caruthers. 1977. Binding of synthetic lactose operator DNAs to lactose repressors. *Proc. Natl. Acad. Sci. USA.* 74:3292–3296.

77. Riggs, A. D., R. F. Newby, and S. Bourgeois. 1970. *lac* repressor-operator interaction II. Effect of galactosides and other ligands. *J. Mol. Biol.* 51:303–314.

78. Riggs, A. D., R. F. Newby, and S. Bourgeois. 1970. *lac* repressor-operator interaction I. Equilibrium studies. *J. Mol. Biol.* 48:67–83.

79. Lin, S. -Y., K. Itakura, J. M. Rosenberg, G. Wilcox, C. Bahl, et al. 1976. Molecular Mechanisms in the Control of Gene Expression D. P. Nielich, W. J. Rutter, and C. F. Fox, editors. Academic Press, New York. 143–158.

80. Dunaway, M., J. S. Olson, J. M. Rosenberg, O. B. Kallai, R. E. Dickerson, et al. 1980. Kinetic studies of inducer binding to *lac* repressor-operator complex. *J. Biol. Chem.* 255:10115–10119.